Prell, W. L., Niitsuma, N., et al., 1991
Proceedings of the Ocean Drilling Program, Scientific Results, Vol. 117

20. PLIOCENE TO PLEISTOCENE VARIATIONS IN CALCIUM CARBONATE, ORGANIC CARBON, AND OPAL ON THE OWEN RIDGE, NORTHERN ARABIAN SEA[1]

David W. Murray[2] and Warren L. Prell[2]

ABSTRACT

Site 722 provides high resolution records of percent $CaCO_3$, magnetic susceptibility, $\delta^{18}O$, organic carbon, and coarse fraction for the past 3.4 m.y. from the crest of the Owen Ridge, northwestern Arabian Sea. Within this time interval, most of the carbonate percent variations can be attributed to terrigenous dilution and do not reflect changes in the carbonate system. From the late Pliocene to Present, the average rate of calcium carbonate accumulation increases from 1 to 3 g/cm^2/k.y. and the average accumulation of organic carbon decreases from 75 to 30 mg/cm^2/k.y. The carbonate component is more dissolved in the older interval. The long-term variations in carbonate accumulation may reflect a greater input of organic matter in the late Pliocene, which decomposes to produce CO_2 and dissolve carbonate. Magnetic susceptibility and % noncarbonate (100 − $CaCO_3$%) reflect changes in the amount of the lithogenic component in the sediments. The period of variation of lithogenic material is the same period as the original forcing of the regional summer monsoon, however, the timing matches global aridity patterns and global ice volume (sea level) changes. This preliminary analysis suggests that the high frequency variation of lithogenic material persists for at least the last 3.4 m.y.

Within the last million years, calcium carbonate accumulation has a large amplitude signal that covaries with major changes in ice volume. Both calcium carbonate and noncarbonate (mostly terrigenous) accumulation are greatest during glacial stages. Interglacial intervals are characterized by low mass accumulation rates, increased foraminifer fragmentation, and increased opal concentration. The accumulation of organic carbon matches the high frequency changes in sedimentation rates. We attribute this high correlation to enhanced preservation of organic carbon by increased sedimentation rate. Of the three major biological components studied, only opal exhibits the variations expected for a biological productivity system forced by monsoonal upwelling driven by changes in northern hemisphere summer radiation.

INTRODUCTION

The northwestern Arabian Sea is one of the world's most productive oceanic areas. The large standing stock of plankton in this region is sustained by seasonal upwelling driven by the strong summer winds associated with the Indian Ocean summer monsoon. Recent studies of foraminifers, pollen, and windborne detritus (Prell, 1984 a, b; Prell and Van Campo, 1986; and Sirocko and Sarnthein, 1989; Clemens and Prell, 1990) indicate that the deep-sea sediments in the northwestern Arabian Sea contain both a terrestrial and oceanic record of the monsoon.

Pelagic sediments on the Owen Ridge lie beneath the area affected by monsoon-driven upwelling and should record long-term variations in the strength of the monsoon. Preliminary Leg 117 shipboard results noted a strong cyclicity in Owen Ridge sediment properties such as color, magnetic susceptibility, wet-bulk density, and calcium carbonate content (Prell, Niitsuma, et al., 1989). Analysis of these data over the upper 100 m reveal a dominant cyclicity of about 1 m or about 23 k.y., the period associated with earth's precessional radiation changes. Previous studies on the large scale features of the monsoon using atmospheric circulation models (Kutzbach and Gütter, 1986; Prell and Kutzbach, 1987) indicate that variations in northern hemisphere summer insolation caused by the cyclic precession of the equinoxes are largely responsible for changes in the strength of the summer monsoon. Encouraged by these results, we examine the major sediment components from the Owen Ridge which are responsible for the cyclic changes in sediment properties to determine whether they record variations in the intensity of the monsoon as indicted by atmospheric circulation simulations.

During the last 3.4 m.y., Owen Ridge sediments reflect a two-component mixture of biogenic calcite and terrigenous materials. Organic matter and biogenic opal together comprise less than 5% of the sediment. Because of this, variations in the input of either calcium carbonate or terrigenous material will directly alter the percent of the other component. The terrigenous material on the Owen Ridge is largely eolian dust from nearby land areas (Sirocko and Sarnthein, 1989; Clemens and Prell, 1990; Clemens and Prell, this volume). Terrigenous input to the deep sea should be controlled by changes in wind direction and strength, and source area aridity. On the other hand, calcium carbonate is mostly derived from the shells of coccolithophores and foraminifers and its input to this supralysoclinal site should be controlled by the balance between surface water production driven by monsoon upwelling and carbonate dissolution resulting from organic matter degradation. In this study we quantify high frequency [up to 1/(12 k.y.)] variations in the concentration and accumulation of calcium carbonate and organic carbon during the past 3.4 m.y. and variations in opal during the past 388 k.y. to determine whether these biological components reflect variations in the intensity of the regional monsoonal upwelling. The 0–3.4 Ma time interval was chosen to include major shifts in global climate (Raymo et al, 1989; Ruddiman et al., 1989). Because terrigenous concentration variations can be inferred from the inverse of the carbonate changes, we also discuss relative changes in the terrigenous component. Clemens and Prell (this volume) provide a more detailed study of the timing of terrigenous flux and grain size variations of the terrigenous silt sized component over the past million years.

[1] Prell, W. L., Niitsuma, N., et al., 1991. *Proc. ODP, Sci. Results*, 117: College Station, TX (Ocean Drilling Program).

[2] Department of Geological Sciences, Brown University, Providence, RI 02912, U.S.A.

DATA AND METHODS

Hole 722B (16°37.3′N, 59°47.8′E; 2027 m water depth) was chosen for the construction of a composite record of sediment deposition on the Owen Ridge for the past 3.4 m.y. (Fig. 1). Compared to the other five holes drilled in the late Neogene pelagic sequence on the Ridge, Hole 722B contains the most complete record of deposition. High quality shipboard volume magnetic susceptibility (k) data measured at 5-cm intervals provide an excellent data base for detailed hole-to-hole and site-to-site correlations (Prell, Niitsuma, et al., 1989). We use these data to construct the composite depth section for Hole 722B.

For this study, Hole 722B was sampled at 20-cm intervals in Cores 1H through 12X [0.01–105.51 meters below seafloor (mbsf)]. All samples were analyzed for calcium carbonate, organic carbon, and coarse fraction contents, as well as the isotopic composition of *Globigerinoides sacculifera* (300–355 μm). The samples were freeze-dried and then split. Two-thirds of the dried sample was separated for faunal and isotope analysis. The remaining one-third was ground for the chemical analyses.

Calcium carbonate content was measured on a gasometric apparatus similar to that described by Jones and Kaiteris (1983). The Brown University system uses a differential pressure gauge in place of a vacuum gauge and carbonate reactions are measured at atmospheric pressure. Replicate analyses of both samples and standards routinely give an analytical precision of better than 0.5% by weight.

Organic carbon measurements were made on a Carlo Erba NA1500 carbon analyzer after removal of calcium carbonate. We followed the technique described by Verardo et al. (1990) for removal of the inorganic carbon fraction. Dried samples were placed in aluminum sample holders and treated with sulfurous acid (8% reagent grade) until the reaction was complete. The residue was then measured for carbon and nitrogen. All analyses were duplicated and the differences were generally less than 5% by weight. The average values are reported in the Appendix.

Opaline silica measurements were made on 10-cm-spaced samples from nearby 15.96 m piston core RC27-61 (16°39.5′N, 59°31.4′E; 1893 m water depth) (Fig. 1). This core spans the same time interval as the top 20 m of Hole 722B. A hot 2M Na_2CO_3 leach was used to extract opal from the sediment samples. We used the opal extraction technique of Mortlock and Froelich (1989) except that buffered 0.5 M acetic acid, rather than hydrochloric acid, was used to initially remove the carbon-

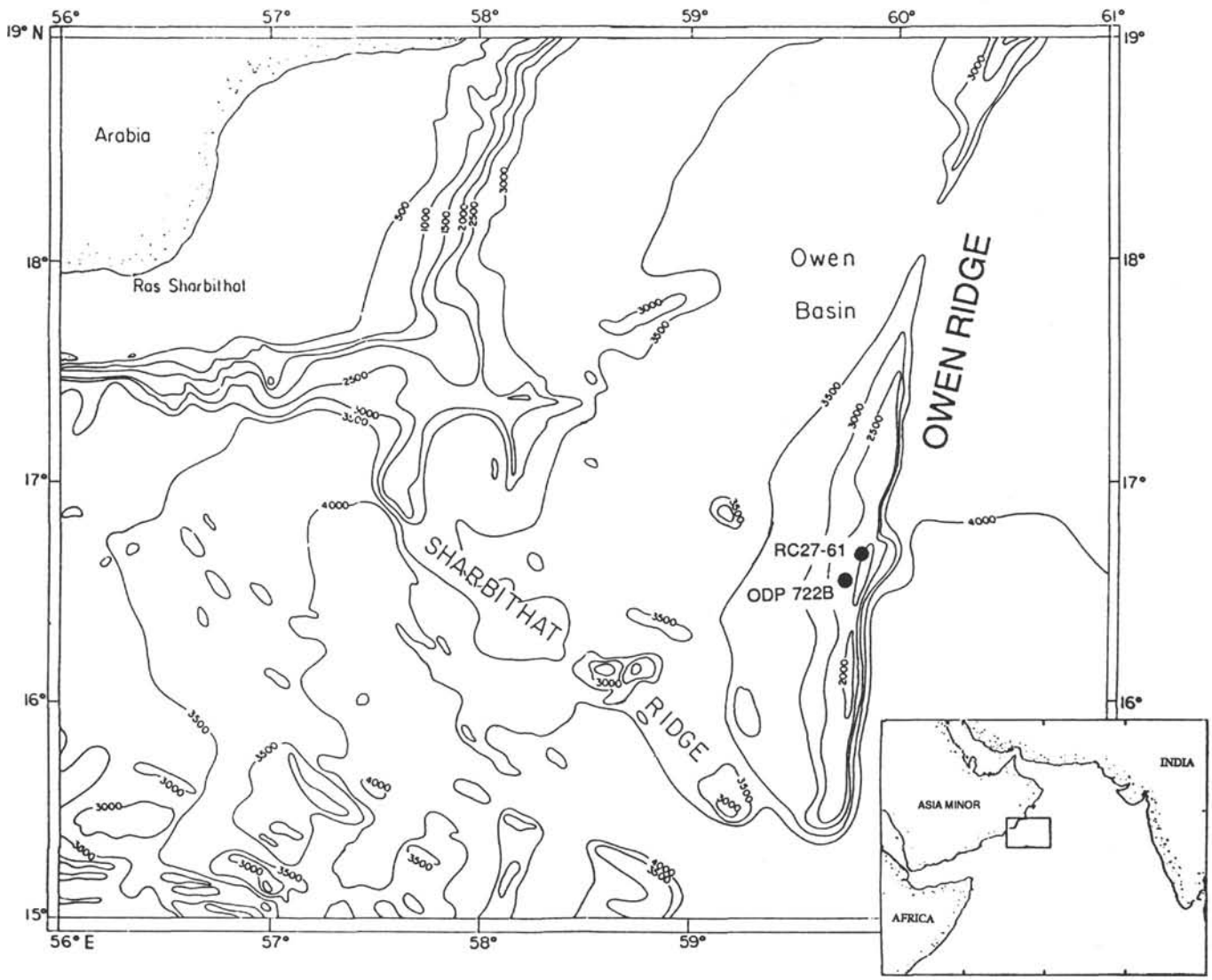

Figure 1. Bathymetric map of Leg 117 operations area and location of ODP Hole 722B and piston core RC27-61. Contours in meters.

ate fraction. Measurements were made on a Beckman DU spectrophotometer and the precision based on replicates was within ± 2%.

Dry bulk density data needed to determine mass accumulation rates were derived from the shipboard GRAPE wet bulk density measurements. Hole 722A shipboard GRAPE data (1.8-cm-spaced measurements) was first smoothed with a cubic spline and then sampled at depths corresponding to the discrete shipboard bulk density measurements for the top 100 m. A linear regression based on GRAPE wet bulk density (GWBD) and discrete shipboard dry bulk density (DBD) data [DBD = −1.2664 + 1.3481 (GWBD); r = 0.84] was used to estimate dry bulk density values for Hole 722B samples. GRAPE values were obtained for individual samples used in this study (Appendix) by linearly interpolating between adjacent 1.8-cm-spaced measurements. GRAPE data gaps due to coring and unmeasured short core sections were filled with data from the offset holes used to construct the composite depth model.

COMPOSITE DEPTH

The core recovery for Hole 722B was excellent within the advanced hydraulic piston cored interval from 0 to 91.9 mbsf (>100%, Prell, Niitsuma, et al., 1989). However, with detailed hole-to-hole correlations based on magnetic susceptibility measurements, gaps as large as 1.90 m were recognized across core breaks. To ensure that the records were complete before analysis of the time series, we constructed a composite depth model for Hole 722B by splicing in short sections from offset Holes 722A and 721B. Magnetic susceptibility data sampled at 5-cm spacing, together with visual marker layers (Prell, Niitsuma, et al., 1989), were used to correlate the holes and recognize data gaps. Sediments in Holes 721B and 722A provided the necessary material to fill in all missing sections in Hole 722B. Two examples of the between-hole correlations and gaps at core breaks are shown in Figure 2. Based on ODP sub-bottom depths, a 40-cm overlap in depth occurs between Cores 6H and 7H in Hole 722B (Fig. 2A). Compared to the sediment sections cored in Holes 722A and 721B, 1.90 m is missing from Hole 722B. The interval from 51.50 mbsf and 53.65 mbsf in Hole 721B was spliced into the gap between Cores 6H and 7H to obtain the composite section. Similarly, 0.55 m from Hole 721B was added to the base of Core 7H in Hole 722B to account for the missing sediment at the break between Cores 7H and 8H (Fig. 2B).

The composite depth model for Hole 722B was constructed by assigning the sediment-water interface a depth of 0 mbsf and successively adding each spliced sediment section down through the sediment column (Table 1). This follows the approach of Ruddiman et al. (1989) in their construction of a composite depth model for DSDP Sites 607 and 609. However, this technique violates the original ODP shipboard depths by continuously adding to the reported sub-bottom core depth. A potential problem is apparent in Figure 2B where the resulting sub-bottom depth in the composite depth model is substantially greater than the true depth below seafloor. The increase in magnetic susceptibility near 66 mbsf in Hole 722B is within 0.5 m of depth below seafloor for this event in the other two holes. However, in the composite depth model, the new depth of this event is almost 3.5 m greater. A total of 5.80 m was added to the top

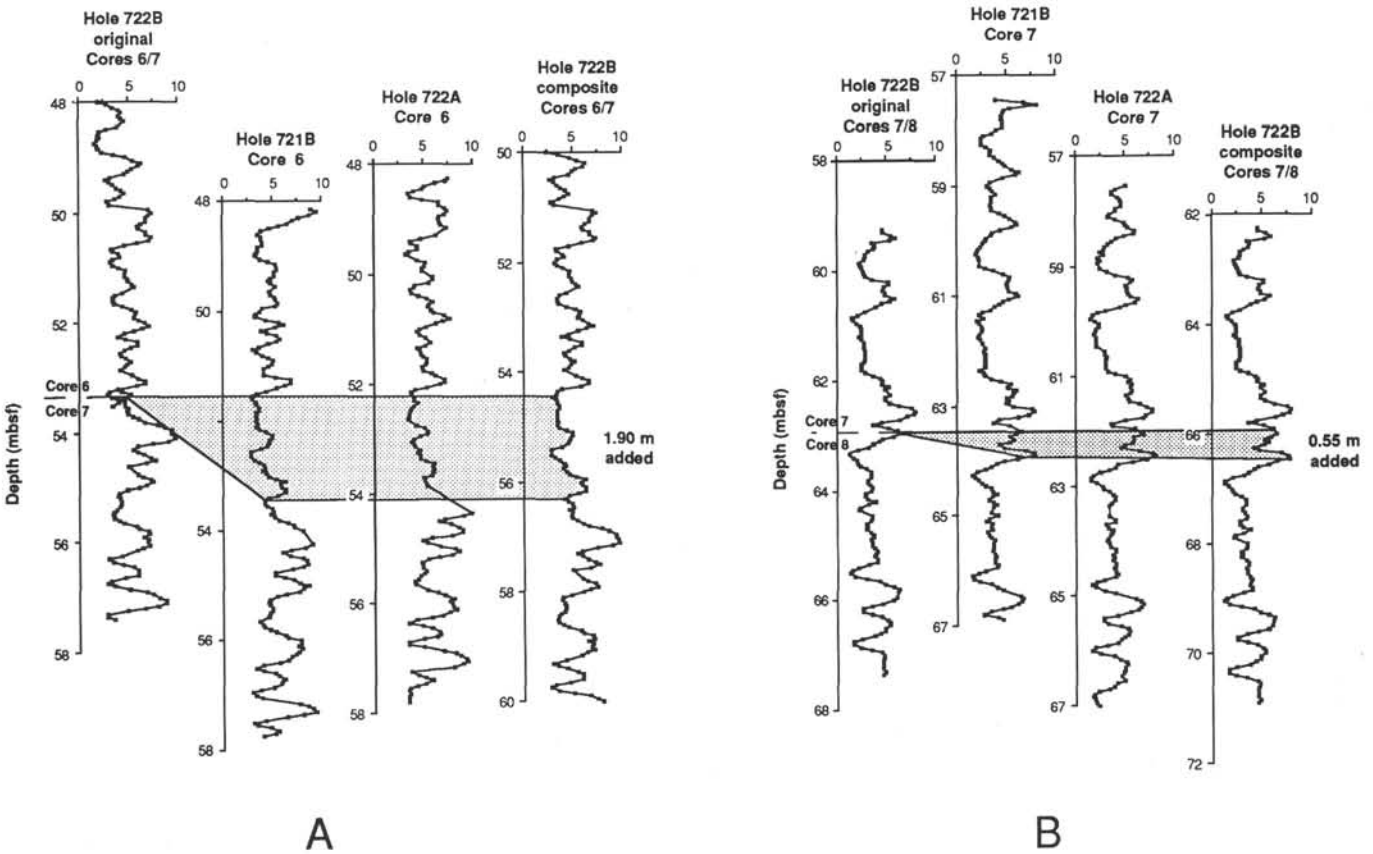

Figure 2. Hole-to-hole correlation and composite volume magnetic susceptibility (10^{-6} cgs) record for the gaps between **(A)** Cores 6 and 7 and **(B)** Cores 7 and 8 in Hole 722B. The shaded portion in each diagram indicates the sedimentary section missing from Hole 722B that is added to the composite depth model.

Table 1. Composite depth model for Hole 722B.

From sample	To sample	Original depth (mbsf) From	To	Composite depth (mbsf) From	To
722B-1H-1, 1 cm	1H-4,19 cm	0.01	5.19	0.01	5.19
722A-1H-3, 80 cm	1H-3, 130 cm	3.80	4.30	5.20	5.70
722B-2H-1, 21 cm	2H-7, 9 cm	5.71	14.59	5.71	14.59
722A-2H-3, 90 cm	2H-4, 34 cm	13.70	14.64	14.60	15.54
722B-3H-1, 45 cm	3H-7, 54 cm	15.45	24.64	15.55	24.74
721B-3H-4, 25 cm	3H-4, 130 cm	23.85	24.90	24.75	25.80
722B-4H-1, 86 cm	5H-7, 59 cm	25.56	43.89	25.81	44.14
721B-5H-3, 30 cm	5H-3, 120 cm	41.80	42.70	44.15	45.05
722B-6H-1, 6 cm	6H-7, 34 cm	43.96	53.24	45.06	54.34
721B-6H-3, 40 cm	6H-4, 105 cm	51.50	53.65	54.35	56.45
722B-7H-1, 26 cm	7H-3, 150 cm	53.46	57.65	56.46	60.70
[a]721B-H-1, 75 cm	7H-2, 60 cm	58.15	59.50	60.85	62.20
722B-7H-5, 1 cm	7H-7, 70 cm	59.25	62.90	62.21	65.90
721B-7H-4, 146 cm	7H-5, 54 cm	63.36	63.94	65.91	66.49
722B-8H-1, 5 cm	8H-7, 64 cm	62.95	72.54	66.50	76.09
721B-8H-4, 130 cm	8H-5, 55 cm	72.70	73.45	76.10	76.85
722B-9H-1, 11 cm	9H-7, 79 cm	72.61	82.29	76.86	86.54
721B-9H-5, 80 cm	9H-6, 45 cm	83.20	84.35	86.55	87.70
722B-10H-1, 11 cm	10H-7, 69 cm	82.81	92.39	87.71	97.29
721B-10X 6, 20 cm	10X-6, 110 cm	94.20	94.60	97.30	97.70
722A-10X-3, 90 cm	10X-4, 90 cm	90.40	91.90	97.75	99.25
722B-11X-2, 31 cm	11X-4, 119 cm	93.71	97.59	99.26	103.14
721B-11X-4, 70 cm	11X-6, 20 cm	100.80	103.30	103.15	105.65
722A-11X-3, 40 cm	11X-4, 145 cm	99.60	102.15	105.70	108.25
722B-12X-1, 96 cm	12X-3, 105 cm	102.46	105.55	108.26	111.35

[a] No magnetic susceptibility data available for Section 722B-7H-4.

of Core 12X because of material spliced in at core breaks in the preceding intervals. Alternatively, we could have preserved the original depths of each core and linearly squeezed the composite section to fit within the reported ODP core length. This is much more difficult to document and causes a nonuniform adjustment of sub-bottom depth for individual sediment samples. Our composite depth reconstruction for Hole 722B Cores 1H through 12X is documented in Figure 3 and Table 1. The sediment thickness added at each core break are listed in Table 2, and composite depths for individual samples are listed in the Appendix.

The magnetic susceptibility values assigned to the individual samples used in this study were obtained by linearly interpolating between the 5-cm-spaced measurements of the composite record. As shown in Figure 3, the 20-cm-spaced interpolated record preserves most of the structure of the original signal. Therefore, our 20-cm samples should record the major changes in sediment properties over the interval studied. The interpolated magnetic susceptibility and the noncarbonate portion of the sediment are highly correlated (Fig. 4). We use this relationship to fill in $CaCO_3$% data gaps at core breaks in the composite record of Site 722. A regression between carbonate and magnetic susceptibility with 10 samples above and 10 below each data gap was used to obtain the carbonate values needed for the composite record. This provides a continuous record of the relative changes between calcium carbonate and noncarbonate (terrigenous material) on the Owen Ridge for the past 3.4 m.y. A major shift in the mean variation of magnetic susceptibility is observed near 6.60 mbsf; values from 0 to 6.60 mbsf average 9.97×10^{-6} cgs while values from 6.60 to 105.5 mbsf average 3.69×10^{-6} cgs. This shift, which reflects a relative increase in concentration or size of the magnetic minerals in the Hole 722B sediments since 150 k.y., is not observed in the calcium carbonate concentration data. To avoid the influence of this shift in calculating values for the composite record, we used a regression based on six samples above and below the gap between Cores 1 and 2 to obtain the $CaCO_3$% value at 5.54 m. Composite records of magnetic susceptibility, noncarbonate, and dry bulk density are shown in Figure 5 and listed in the Appendix. As noted earlier, the density values were obtained from interpolated GRAPE data using sections from offset holes to fill data gaps.

AGE MODEL

Shipboard magnetic-reversal stratigraphy was used to provide a preliminary age model for the past 3.4 m.y. of Hole 722B (Table 3). With the exception of the upper limit of *Discoaster pentaradiatus* (2.40 Ma), the nannofossil datums used to determine accumulation rates for the Leg 117 *Initial Reports* (Prell, Niitsuma, et al., 1989) lie along the linear rates between magnetic events (Fig. 6A). This coarse resolution age model provides mean sedimentation rates covering approximately 1 m.y. intervals. In Hole 722B, these rates range from 23 m/m.y. for 2.5–3.4 Ma to 41 m/m.y. for 0–1 Ma.

Oxygen isotope stratigraphy has been used routinely to correlate cores from different oceanic environments and place them in a common chronostratigraphic framework (Imbrie et al., 1984). Compared to oxygen isotopic records from other oceanic areas with relatively constant sedimentation rates (Imbrie et al., 1984), glacial intervals in Hole 722B are expanded and interglacials are compressed. This indicates that the assumption of a constant sedimentation rate between successive magnetic datums is not valid for Owen Ridge sediments and a higher resolution age model is necessary to accurately record temporal changes in the input of major sedimentary components. Oxygen isotope stratigraphy was used to construct a high resolution age model for Hole 722B from 0 to 1 Ma (Clemens and Prell, this volume). This model relies on ages assigned to oxygen isotope events in the SPECMAP stack (Imbrie et al., 1984) for the last 780 k.y. and the tuned stratigraphy of Ruddiman et al. (1989) between 780 and 1000 k.y. We assume a linear sedimentation rate between 50 identified isotope events to derive ages for individual samples. The age-depth plot in Figure 6B show the differences between the two age models for the 0–1 Ma time interval. Differences of more than 60,000 yr are evident below 20 mbsf. The major disparities between the age models and with respect to the chronology of the SPECMAP stack as shown in Figure 7. Note that for the assumption of constant sedimentation to be valid glacial stages would have to span a longer time interval compared to interglacial stages. The adjustments made by the correlation to the SPECMAP stack requires sedimentation rate to be greater in the glacial stages compared to interglacials. Sedimentation rates (S) for the individual samples (i) were derived from the difference in age (T) and depth (D) of adjacent samples: $S_i = (D_{i+1} - D_{i-1})/(T_{i+1} - T_{i-1})$.

RESULTS

Calcium carbonate is the dominant sediment component at Site 722, accounting for 66 wt% of the sediments during the past 3.4 m.y. In general, interglacial periods are carbonate-rich and glacial stages are carbonate-poor. The $CaCO_3$% and interpolated magnetic susceptibility data exhibit the same scale of variation but are inverse (Fig. 4). This implies that magnetic susceptibility accurately records variations in the noncarbonate component (mostly terrigenous material). We express the calcium carbonate variations in terms of mass accumulation (MAR) to remove the affect of terrigenous dilution; where MAR ($g/cm^2/k.y.$) = concentration (g/g) × sedimentation rate ($cm/k.y.$) × dry bulk density (g/cm^3). High resolution sedimentation rates in Hole 722B are required to quantify high frequency changes in accumulation rate (Fig. 7). Otherwise, a constant sedimentation rate applied to million-year intervals in Hole 722B only captures the changes in accumulation rate at periods longer than 1 m.y. Calcium carbonate accumulation, as quantified with the high resolution oxygen isotope age model, varies from about 1 to 6 $g/cm^2/k.y.$ over the past 1 m.y. These changes are out of phase

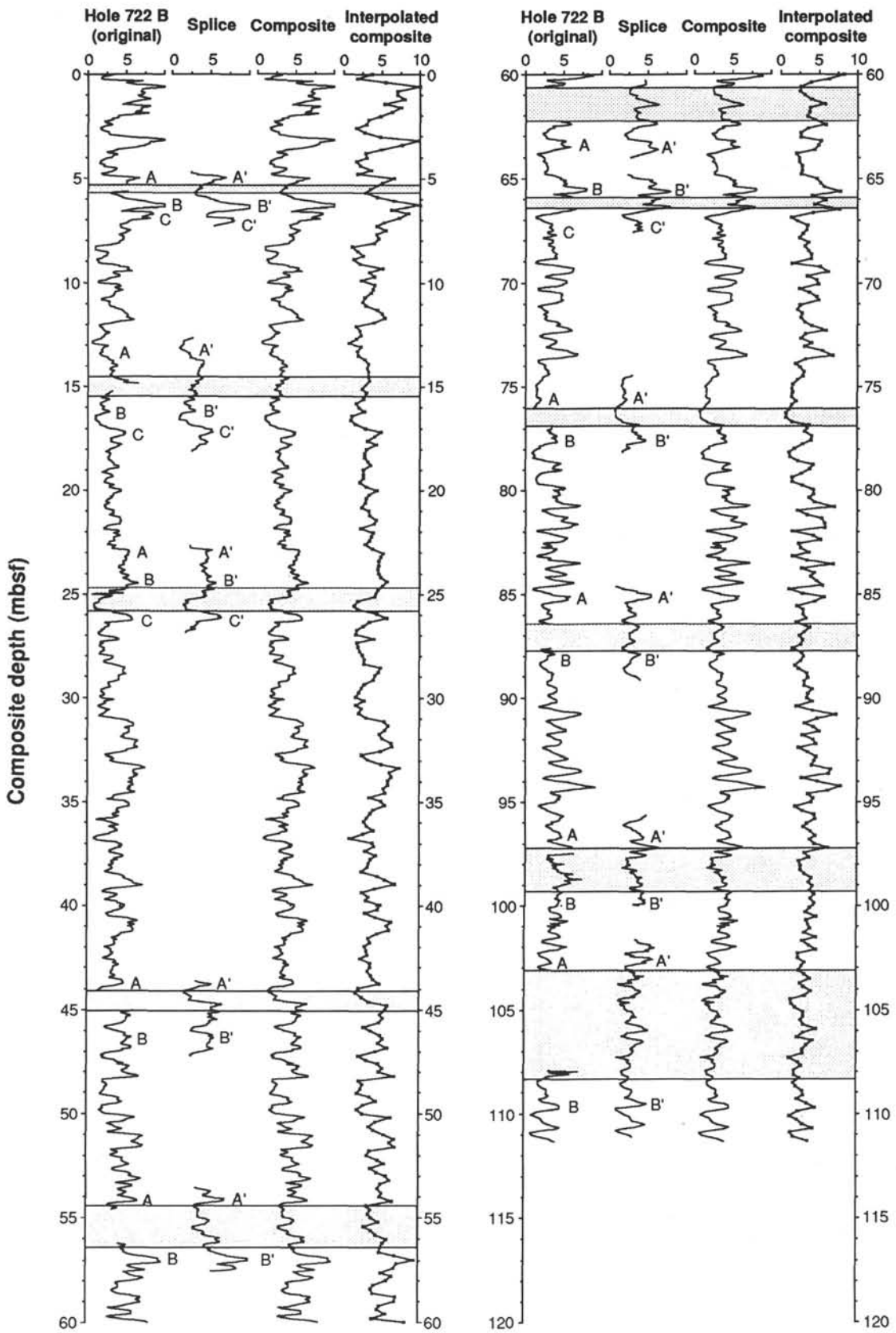

Figure 3. Hole 722B original and composite volume magnetic susceptibility (10^{-6} cgs) records for Cores 1H-12X. Spliced sections used to fill data gaps and suspect intervals (shaded) were obtained from offset Holes 722A and 721B. Magnetic susceptibility data interpolated at depths corresponding to samples analyzed in this study (~20-cm intervals) is shown.

Table 2. Adjusted core-top depths for Hole 722B.

Core	ODP depth (mbsf)	Composite depth (mbsf)	Added depth (m)	Shipboard corrected depth[a] (mbsf)
1H	0.00	0.00	—	0.00
2H	5.51	5.51	0.00	5.80
3H	15.10	15.10	0.00	15.40
4H	24.70	24.95	0.25	25.50
5H	34.30	34.55	0.00	35.30
6H	43.90	45.00	0.85	45.00
7H	53.20	56.20	1.90	55.60
8H	62.90	66.45	0.55	65.50
9H	72.50	76.75	0.70	75.50
10H	82.70	87.60	0.65	84.30
11X	91.90	97.45	0.65	94.10
12X	101.50	107.30	0.25	103.60

[a] From Shipboard Scientific Party (1989, Table 14).

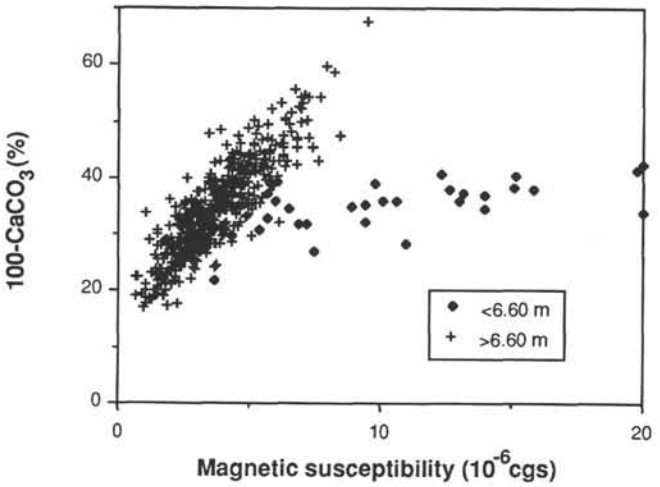

Figure 4. Noncarbonate percent vs. interpolated magnetic susceptibility for Cores 1H–12X in Hole 722B. The division at 6.60 m reflects a shift in the mean magnetic susceptibility values that is not observed in the $CaCO_3$% data.

with the carbonate percent variations. In fact, the 434,000-yr record from nearby piston core RC27-61 shows that high carbonate concentrations associated with interglacial stages correspond to intervals with substantially larger numbers of planktonic foraminifer fragments and lower carbonate accumulation rates as compared to glacial intervals (Fig. 8). These results indicate that the carbonate-rich interglacial intervals are more dissolved than the glacial-aged intervals characterized by lower $CaCO_3$%. Since the site is well above the lysocline, this dissolution may be driven by the degradation of organic matter. Much of the percent variation is due simply to terrigenous dilution, so $CaCO_3$% is not an accurate monitor of the carbonate system at this site. However, the noncarbonate concentration record, which is highly correlated to magnetic susceptibility, provides a reliable monitor of the timing of the input and accumulation of terrigenous material; i.e., greater terrigenous accumulation during glacial stages (Clemens and Prell, this volume).

Opal and organic carbon are only minor components of the Owen Ridge sediments. During the past 388,000 yr, opal varies from about 0.5% to 2.5% and distinct maxima occur within interglacial stages (Fig. 8). Radiolarian shells are the dominant siliceous component in these sediments and diatom remains are

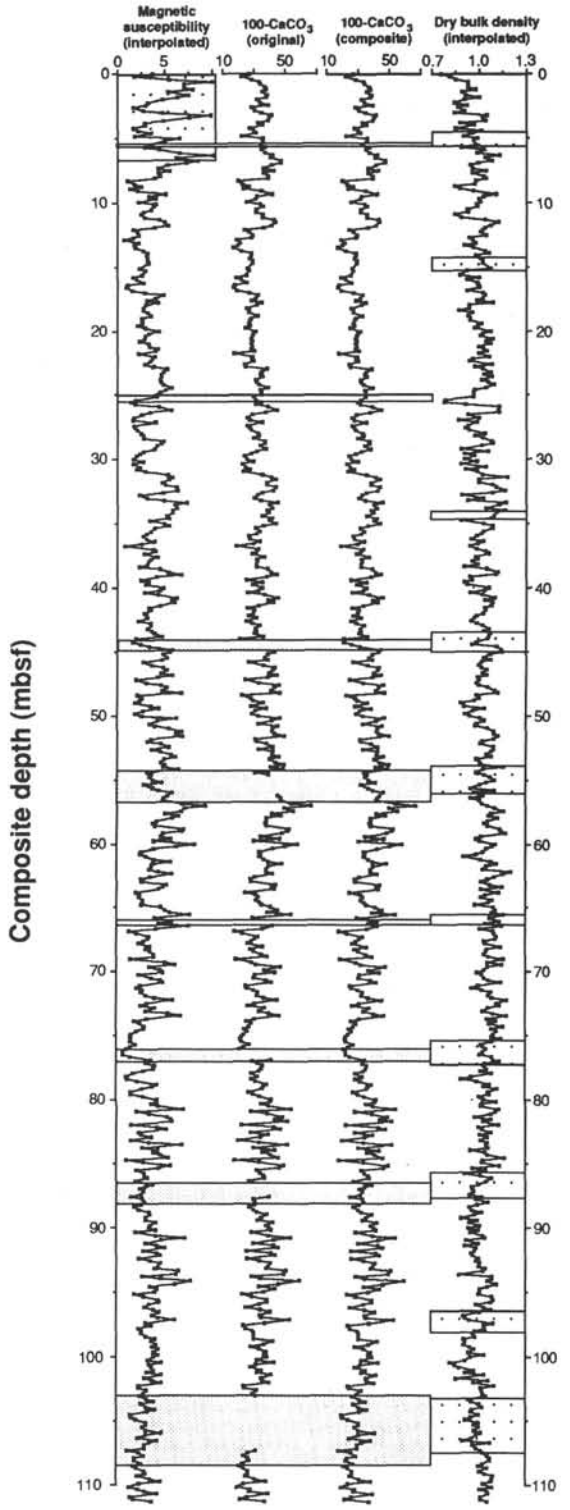

Figure 5. Interpolated magnetic susceptibility (10^{-6} cgs), measured and composite noncarbonate percent, and interpolated dry bulk density (g/cm^3) vs. composite depth for Hole 722B. Shaded intervals indicate data gaps and suspect values where composite noncarbonate values were obtained from a regression between noncarbonate and interpolated magnetic susceptibility data. Magnetic susceptibility data highlighted with the dotted pattern have been divided by two to account for the shift in magnitude near 6.60 m. Spliced dry bulk density data from offset holes are indicated with a dotted pattern.

Table 3. Magnetic and nannofossil datums for Hole 722B.

Event[a]	Age (m.y.)	Composite depth[b] (mbsf)
B *Emiliania huxleyi*	0.19	7.95
T *Pseudoemiliania lacunosa*	0.49	18.90
T *Reticulofenestra* sp. A	0.82	34.65
B Jaramillo	0.98	40.35
T *Calcidiscus macintyrei*	1.45	55.55
T *Discoaster brouweri*	1.90	69.50
T *Discoaster pentaradiatus*	2.40	80.05
Matuyama/Gauss	2.47	89.40
Gauss/Gilbert	3.40	110.80

[a] From Shipboard Scientific Party (1989, Tables 4 and 7).
[b] The hole-to-hole correlation based on magnetic susceptibility was used to obtain Hole 722B composite depths for the nannofossil datums that were originally identified in Hole 722A.

only present in the intervals of highest opal concentrations. The measured opal concentrations within Stage 5 are lower than other interglacial stages. This interval corresponds to large numbers (1.8×10^4/g) of radiolarian shells but no diatoms. The low opal values may be due, in part, to incomplete digestion of the more resistant radiolarian opal by the Na_2CO_3 leach. The opal% variations in RC27-61 are of similar amplitude and are coincident with variations of Si/Al from Hole 722B (Schimmeld et al., this volume). This similarity indicates that opal accounts most of the Si in excess of that associated with the detrital aluminosilicate component. Opal accumulation in core RC27-61 generally exhibits the same temporal pattern as the concentration data (Fig. 8). The average rate of accumulation (19 mg/cm^2/k.y.) for the past 388 k.y. is close to that measured in low accumulation rate sediments beneath the eastern equatorial Pacific zone of high productivity (Fischer et al., 1986). We note, however, that the opal accumulation rates on the Owen Ridge are characteristically low for sites with high surface productivity and sedimentation rates of 3–4 cm/k.y.

Organic carbon concentration varies from 0.4% to 2.0% over the past 1 m.y. Preliminary shipboard results indicate that much of the recent organic matter accumulating on the Owen Ridge is of marine origin (Prell, Niitsuma, et al., 1989). Organic carbon accumulation varies from 10.0 to 155 mg/cm^2/k.y. with a mean of 46 mg/cm^2/k.y. for the past 1 m.y. (Fig. 7). This burial rate is significantly higher than that commonly associated with pelagic carbonates and is comparable to mid-water sites on the northwest African and Peru margins (Sarnthein et al., 1989). Glacial intervals are periods of enhanced organic carbon accumulation, greater sedimentation rates, but weaker monsoons. If the amount of organic carbon production is associated with monsoon-driven upwelling then our data suggest that much of the variation in organic carbon accumulation over the last 1 m.y. can be attributed to sedimentation rate enhanced preservation and does not reflect changes in the primary input of organic carbon to the sediments.

The long-term variations in calcium carbonate and organic carbon accumulation, and coarse fraction percent (mostly shells of foraminifers) are shown in Figure 9. We also show the high

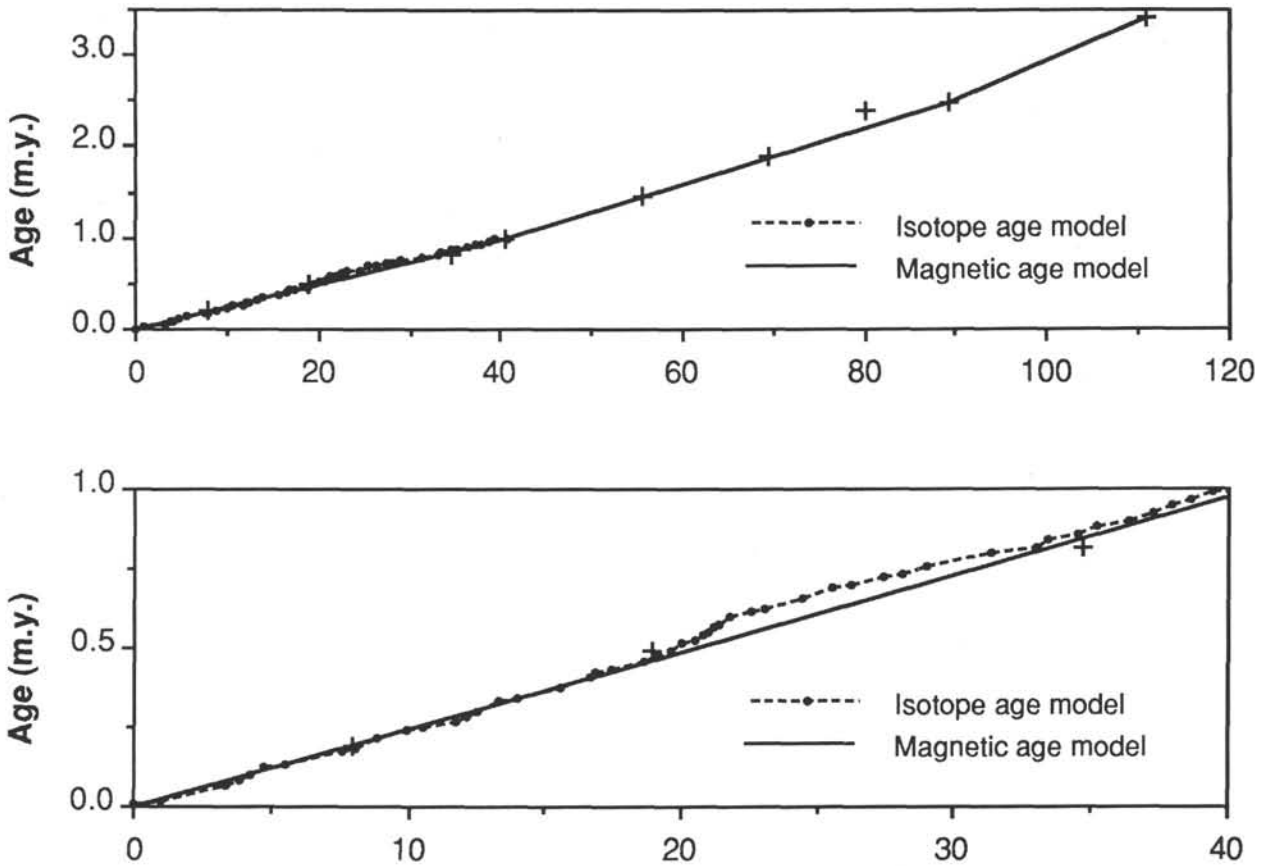

Figure 6. Age vs. depth plots for Hole 722B for 0–120 m (Cores 1H–12X) (top) and 0–40 m (bottom). Pluses are the nannofossil and magnetic reversal datums listed in Table 3. Solid circles are the 50 events used to construct the oxygen isotope-based chronology. See text for discussion of age models.

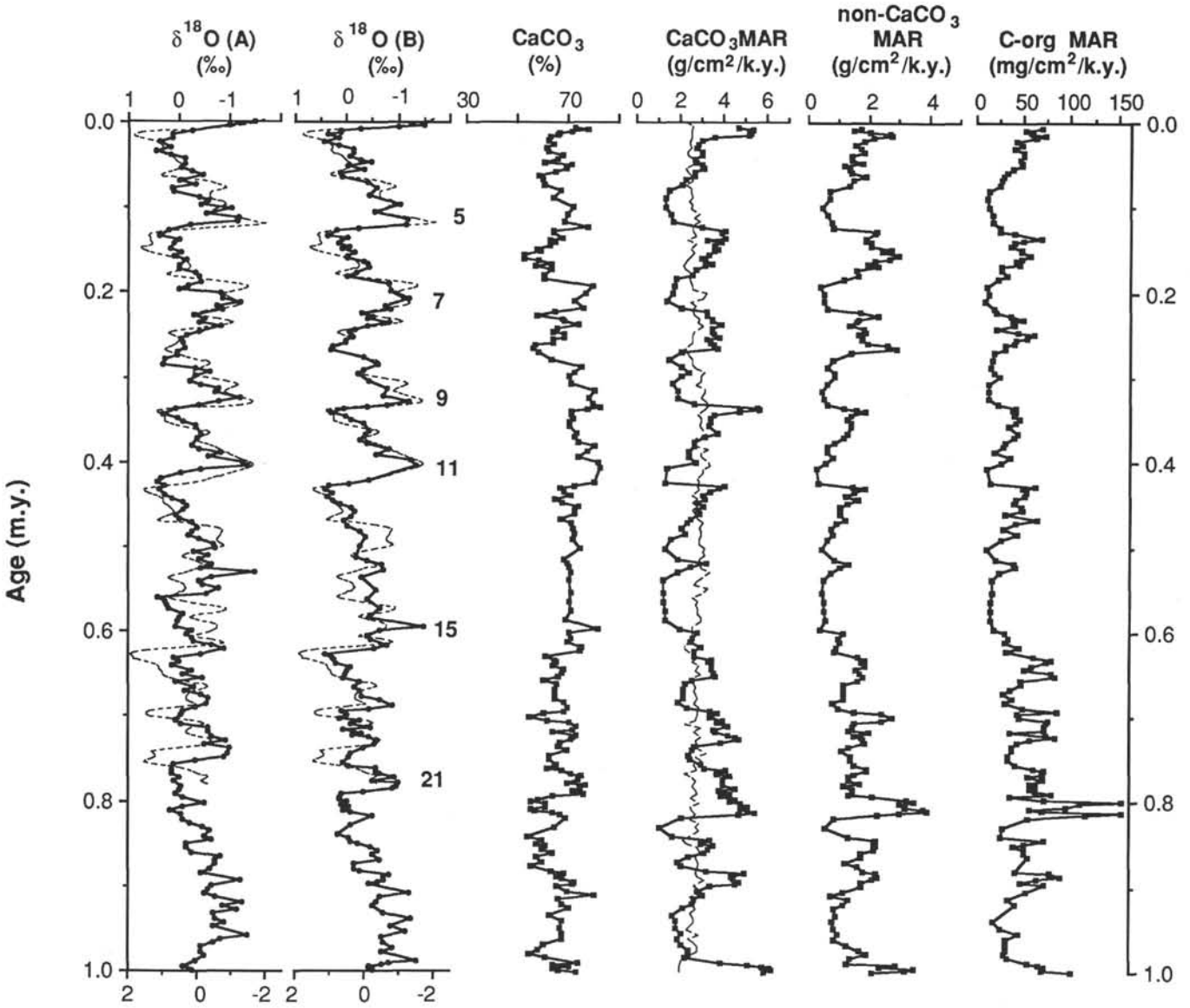

Figure 7. Oxygen isotope composition of *G. sacculifer*, carbonate percent, carbonate MAR, noncarbonate MAR, and organic carbon MAR time series from Hole 722B. The two oxygen isotope profiles reflect differences between chronologies based on **(A)** magnetostratigraphy and **(B)** isotope stratigraphy. For comparison, the thin dashed line on each time series is the SPECMAP stacked isotope record of (Imbrie et al., 1984). Interglacial stages 5–21 are noted. The $CaCO_3$% and the mass accumulation rate profiles (solid line) use the isotope-based chronology and the thin dashed line for the $CaCO_3$ MAR time series relies on the magnetic reversal age model.

frequency variations in MAR calculated with sedimentation rates derived from the isotope age model. This emphasizes the fact that only average or long-terms trends in the MAR's can be determined with a low resolution age model at Site 722. The Pliocene section that begins near 3.4 Ma is characterized by low $CaCO_3$ fluxes of about 1 g/cm^2/k.y. This rate increases by a factor of three from the late Pliocene to Present.

Organic carbon accumulation exhibits more variable changes over the last 3.4 m.y. (Fig. 9). Between 2.8 and 3.4 Ma, the average rates were low and close to present values of 20–30 mg/cm^2/k.y. The accumulation rates then increase after 2.8 Ma to a maximum of 125 mg/cm^2/k.y. near 2.4 Ma. This increase in organic carbon accumulation precedes the rise in calcium carbonate accumulation near 2.4 Ma. The average organic carbon MAR decreases from the late Pliocene to Pleistocene with present values near 30 mg/cm^2/k.y. for the top of the Owen Ridge. Since the high carbon accumulation rates near 2.4 Ma are associated with an interval of lower mean sedimentation rate compared to the Present, the high rates in the late Pliocene cannot be attributed to sedimentation rate enhanced preservation. This implies that oceanographic conditions were more favorable for organic carbon production in the late Pliocene compared to the present, due either to the local influence of monsoonal upwelling or regional oceanographic changes which provide more nutrients to the surface waters. These changes are also noted in the nearby sites on Oman Margin (Prell, Niitsuma, et al., 1989). The margin sites are characterized by laminated sediments with increases in opal and organic carbon over the interval from 1.5 to 3.4 Ma. The presence of laminae at the margin sites implies that the oxygen minimum zone was intensified during the late Pliocene.

Coarse fraction (>150 μm) weight percent exhibits a trend similar to the carbonate mass accumulation rate and inverse to the organic carbon profile. The coarse fraction is mostly com-

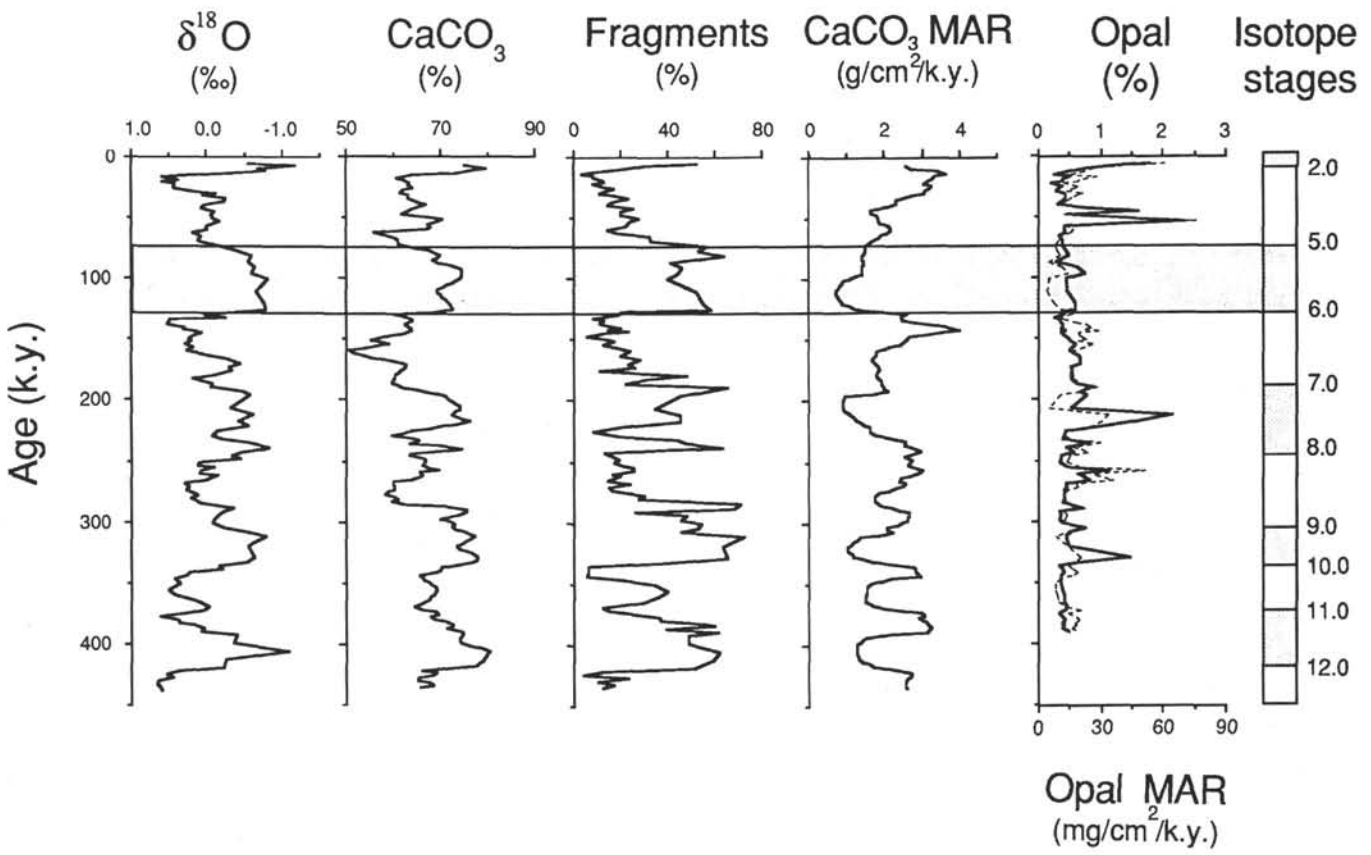

Figure 8. Time series of $\delta^{18}O$, $CaCO_3$%, foraminifer fragments, calcium carbonate mass accumulation rate, opal percent, and opal accumulation for the upper 12.96 m of piston core RC27-61. Oxygen isotope stages are shown for reference and interglacial stage 5 is highlighted.

posed of calcite, and the low values prior to 1.5 Ma suggest that the older samples are more dissolved than younger material. This pattern is consistent with more organic carbon production in the late Pliocene compared to the present. Upon decomposition, the organic carbon will produce CO_2 which enhances carbonate dissolution. A more detailed analysis of the amplitude and timing of these events awaits a high resolution age model for the interval older than 1 Ma.

DISCUSSION

The 3.4 m.y. time series of bulk changes in sediment composition on the Owen Ridge (Figs. 5 and 9) reveal a high frequency scale of variation close to 23 k.y. (i.e., the period associated with changes in the earth's precession cycle). We focus our discussion on the significance of the dominant periods of change and the relative timing among the sedimentary components considered in this study. Standard time series analysis (Jenkins and Watts, 1968) is used to quantify these relationships. As noted previously, noncarbonate (100 – $CaCO_3$%) and magnetic susceptibility reflect the terrigenous percent changes and match temporal variations in terrigenous accumulation during the past 1 m.y. (see Clemens and Prell, this volume). Therefore, $CaCO_3$% can be used to determine the dominant period of variation of the lithogenic component. Because of the large variation in sedimentation rate between glacial and interglacial stages, spectra for the interval from 0 to 1 Ma differ depending on whether we use a coarse or high resolution age model (Fig. 10). Using the oxygen isotope-based chronology, $CaCO_3$% variance is concentrated in the 100, 41, and 23 k.y. bands that are common in deep-sea paleoclimatic records and associated with astronomical-forced changes in climate (Fig. 10A). The accumulation record also has concentrations of variance in the orbital bands, but the low frequency bands dominate. This may be due, in part, to our inability to resolve high frequency variations in sedimentation rate in the Hole 722B record (Clemens and Prell, this volume). Similar periods are present in the records of calcium carbonate concentration (Fig. 10B) and accumulation (Fig. 10D) with the low resolution magnetic reversal based chronology (Fig. 10B), but substantial differences exist in the distribution of variance. To avoid these errors resulting from inaccuracies in the low resolution age model, we focus our discussion on the record from the last 1 m.y. where a high resolution chronostratigraphy is available.

Within the last 1 m.y., most of the time series considered in this study contain one or all three of the frequency bands associated with astronomical-forced changes in climate. We use cross spectral analysis to better understand the relationships among the major sediment components and to compare their temporal changes to global and regional climatic variations. All time series are compared to an orbital curve referred to as ETP (Imbrie et al., 1984), and the results of the phase spectrum in the orbital bands are summarized in Table 4. The ETP curve is derived by normalizing and then summing time series of eccentricity (100 k.y.), obliquity (41 k.y.), and (negative) precession (23 k.y.). The resulting curve contains the relative amplitude and phase of all frequencies associated with the orbital variations.

Previous time series analysis of Owen Ridge sediments by Prell (1984a) noted that the record of *Globigerina bulloides,* which is used as an upwelling index in the Arabian Sea, is coherent with 23 k.y. precessional changes. This result and subsequent work by Prell and Kutzbach (1987) confirm that variations in solar radiation are the primary forcing for the regional monsoon circulation during the late Quaternary. However, a significant lag of 5–9 k.y. exists between the proposed forcing

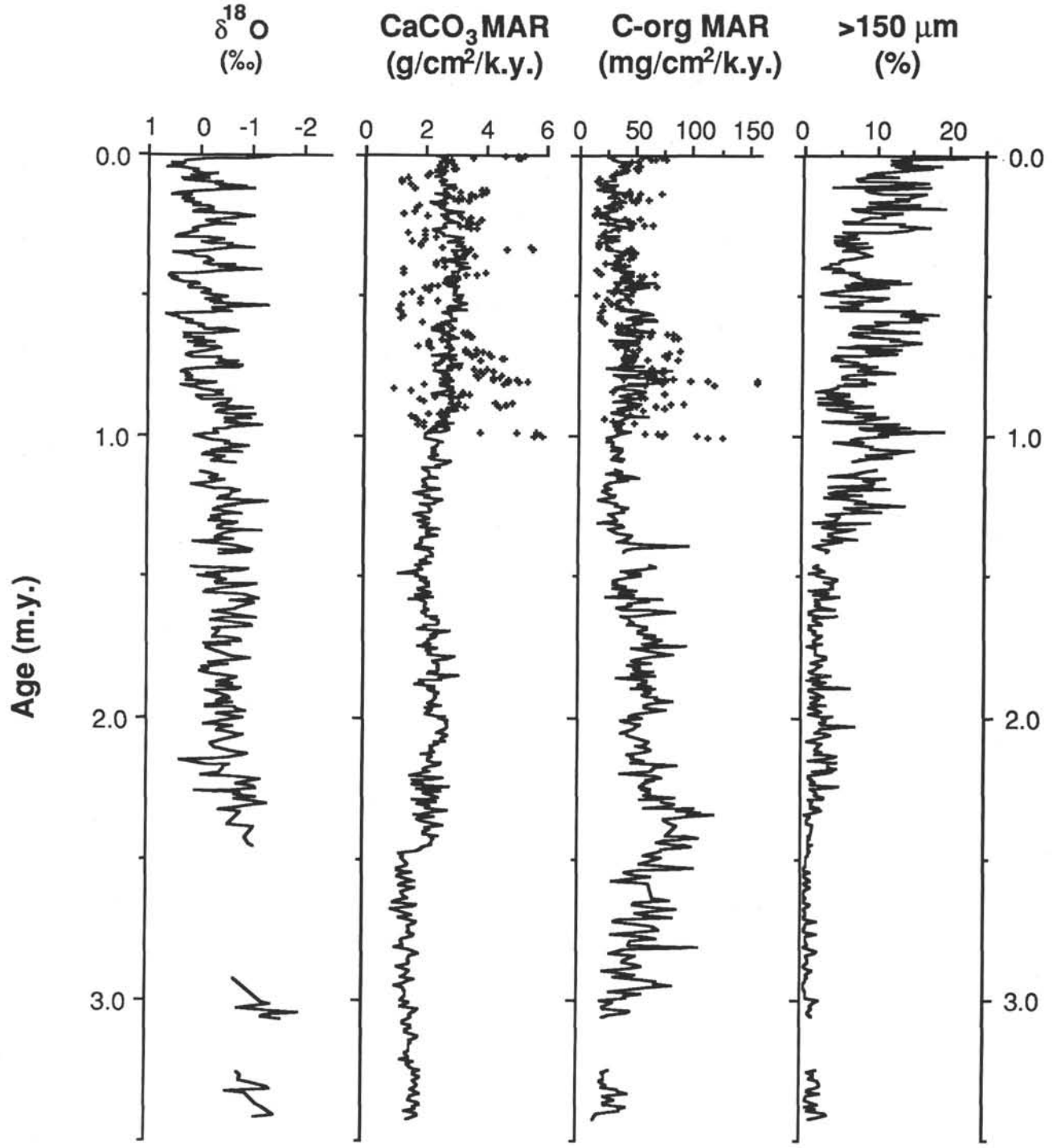

Figure 9. Time series of planktonic $\delta^{18}O$ (‰), calcium carbonate and organic carbon mass accumulation rates, and coarse fraction (>150 μm) from Hole 722B composite data. The ages for the isotope data are derived from the low resolution magnetic reversal chronology. Data represented by the solid lines in the MAR profiles use chronologies based on magnetic stratigraphy and the pluses represent values calculated using the oxygen isotope based age model.

(maximum precessional radiation referenced to June 21) and indices of monsoon strength (Prell, 1984a; Prell and Kutzbach, 1987; Clemens and Prell, this volume). This lag suggests that internal feedbacks within the climate system are necessary to explain the observed temporal variations preserved in the deep-sea record. Conceptual models which consider these feedbacks are discussed by Prell (1984a) and Clemens and Prell (1990).

The time series of the oxygen isotopic composition of *Globigerinoides sacculifer* is coherent and in phase with the SPECMAP stack within each of the orbital bands over the intervals common to both records. This indicates that our age model is reliable and phase differences between other sediment indices and the ETP time series within the orbital bands cannot be attributed to inaccuracies in the age model. The reported phases

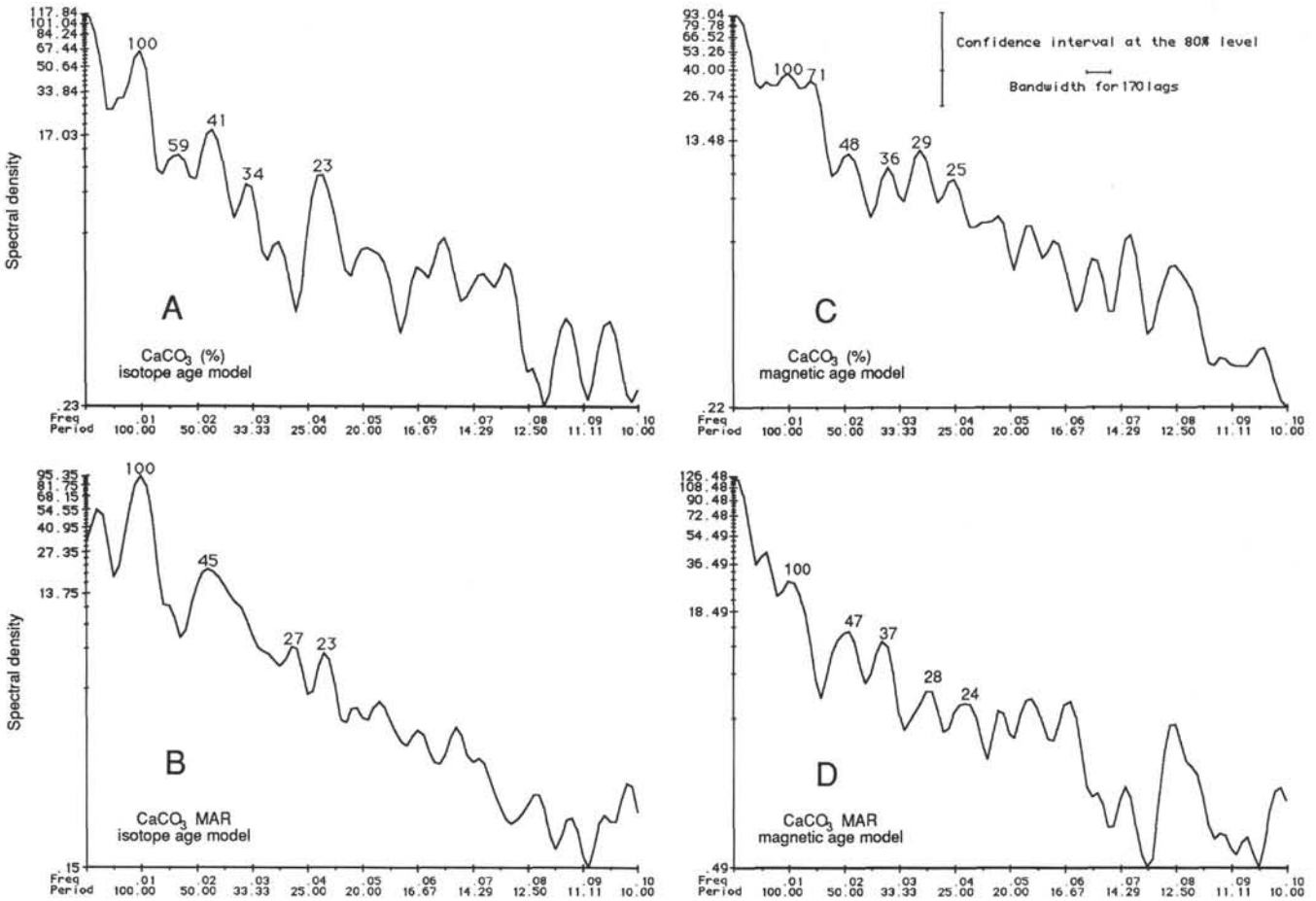

Figure 10. Variance spectra of Hole 722B $CaCO_3$% and MAR data from 0 to 1000 k.y. using (**A** and **C**) the oxygen isotope- and (**B** and **D**) the magnetic reversal-based chronologies. Spectra are plotted on a linear frequency scale and a log variance density scale. The bandwidth and the confidence interval for the 80% level are shown.

Table 4. Summary of cross spectral analysis.[a]

Time series[a]	100 k.y. Phase	100 k.y. Coherency	41 k.y. Phase	41 k.y. Coherency	23 k.y. Phase	23 k.y. Coherency
$-\delta^{18}O$ (‰) (min ice)	$-7\pm15°$	0.86	$-79\pm8°$	0.93	$-84\pm11°$	0.92
$CaCO_3$ (%)	$+13\pm15°$	0.64	$-48\pm21°$	0.76	$-76\pm9°$	0.95
Mag. susceptibility	$-180\pm28°$	0.66	$+144\pm26°$	0.69	$+72\pm18°$	0.81
$CaCO_3$ MAR	$+116\pm22°$	0.74	—	—	—	—
non-$CaCO_3$ MAR	$+135\pm25°$	0.70	$+144\pm27°$	0.66	—	—
C-org (%)	$+173\pm26°$	0.69	—	—	$+138\pm27°$	0.66
C-org MAR	$+133\pm22°$	0.74	—	—	$+94\pm23°$	0.74
Opal (%)	—	—	$-12\pm17°$	0.85	$-132\pm9°$	0.94
Opal MAR	$+156\pm30°$	0.65	$+31\pm15°$	0.87	$-128\pm10°$	0.94

[a] Summary of phase spectra between Hole 722B time series and ETP for Milankovitch frequency bands. Positive values indicate that the record leads ETP, and negative values indicate a lag. For all cross spectra but RC27-61 opal% and MAR: record length = 6–1000 k.y.; sample interval = 2 k.y.; # of lags = 170; bandwidth = 0.004; and the test statistic for nonzero coherency at the 80% confidence level = 0.65. For opal% and MAR: record length = 6–388 k.y.; sample interval = 2 k.y.; # of lags = 75; bandwidth = 0.009; and the test statistic = 0.69.

of the oxygen isotope record relative to ETP are consistent with the time constant for changes in ice volume (Imbrie et al., 1984). Since Pleistocene ice volume controls global changes in sea level, the phases also reflect the relative timing of maximum sea level.

In general, $CaCO_3$% is in phase and highly correlated with ice minimum/sea level maximum, and 180° out of phase with the lithogenic component as represented by the magnetic susceptibility and noncarbonate accumulation records (Table 4). Although these 0–1 Ma time series of the lithogenic component exhibit a strong concentration of variance at 23 k.y., which accounts for much of the documented compositional changes in the preliminary shipboard results (Prell, Niitsuma, et al., 1989), the timing is not consistent with indices of monsoon wind strength. In fact, lithogenic concentration and accumulation are at a maximum during glacial intervals (minimum ice phase—

180°; Table 4) when the monsoon circulation is thought to be weakest (Prell and Kutzbach, 1987). The process(es) responsible for the positive association of maximum terrigenous concentration and accumulation with minimum sea level/maximum glacial conditions is discussed in detail by Clemens and Prell (1990).

Calcium carbonate accumulation is only coherent with ETP within the 100 k.y. band and is greatest during the maximum rate of sea-level rise. This site is above the regional lysocline, which lies at approximately 3400 m (Cullen and Prell, 1984), so the accumulation may reflect carbonate productivity. However, the phase relationship is not consistent with other indices of monsoon strength (Prell and Kutzbach, 1987; Clemens and Prell, 1990). This implies that if the changes are due to carbonate productivity in this area, they are not linked in a simple manner to monsoon-induced upwelling. The phase of maximum carbonate accumulation does correspond to the least amount of foraminifer fragmentation in the 434,000 yr record from RC27-61. In addition, the low frequency changes in carbonate accumulation at Site 722 are in phase with the record of lysocline variations from the equatorial Indian Ocean (Peterson and Prell, 1985) where maximum dissolution corresponds to the maximum rate of sea-level rise. This evidence suggests that during the last 1 m.y., the low frequency variations in carbonate accumulation are driven by dissolution. The shoaling of the regional lysocline in the northern Arabian Sea could result from the high flux of organic carbon associated with this zone of high productivity. From the difference in the average glacial and interglacial rates of carbonate accumulation (4 and 1 g/cm^2/k.y., respectively) we estimate that, as the lysocline shoals, an additional 3 g/cm^2/k.y. is dissolved in the interglacial periods compared to glacial intervals. If carbonate productivity follows variations in the monsoon (i.e., increased flux during interglacials), then the primary flux of carbonate would be greater and the amount dissolved between glacial and interglacial intervals would be even larger. This process would provide an effective transfer of carbon from the surface to intermediate waters during interglacial intervals.

Organic carbon accumulation in the Owen Ridge sediments is highly correlated with the terrigenous component variations which drives sedimentation rate changes in this region (Fig. 9). If the organic carbon component reflects variations in primary productivity, then our results imply that local carbon production does not correspond to temporal changes in the strength of the summer monsoon, as inferred from other sediment indices (Prell and Kutzbach, 1987; Clemens and Prell, 1990). Alternatively, the record of organic carbon accumulation is dominated by sedimentation rate enhanced preservation. Our preliminary attempts to remove the effect of sedimentation rate variations using the empirical relationships established by Müller and Suess (1979) and Sarnthein et al. (1988) do not change the timing of the organic carbon cycles; the greater flux of organic carbon is still associated with glacial intervals and not other indices of monsoon strength. Further work is necessary to resolve these discrepancies.

The temporal changes in opal concentration and accumulation during the past 388,000 yr on the crest of the Owen Ridge are similar to and in phase with other indices of monsoon strength such as *Globigerina bulloides* and terrigenous grain size (Clemens and Prell, 1990). All three monsoon indices exhibit a 5–9 k.y. lag relative to changes in northern hemisphere summer insolation. The sharp increases in opal accumulation reflect intervals of enhanced preservation and are linearly correlated to increased northern hemisphere radiation. However, the amplitude of the opal changes is not simply linked with insolation changes. Our preliminary analysis suggests that the siliceous component of the sediments may be a reliable monitor of variations in the intensity of the monsoon and can be used to evaluate long-term changes in regional imprint of the southwest monsoon in the Arabian Sea.

CONCLUSIONS

This study of the major biogenic components of Pliocene-Pleistocene sediments from the Owen Ridge reveals that percent noncarbonate (mostly lithogenic), organic carbon, opal, and volume magnetic susceptibility vary with periods similar to those expected for a system driven by monsoon upwelling and forced by changes in northern hemisphere insolation. However, only opal exhibits a relative timing consistent with a monsoonal-forced system. Variations in percent calcium carbonate, the major sediment component, result from terrigenous dilution and do not reflect changes in the carbonate system. The factor-of-two increase in the mean rate of calcium carbonate accumulation during the past 3.4 m.y., originally thought to reflect the long-term increase in the strength of the monsoon system, most likely results from greater dissolution of the carbonate component in Pliocene sediments compared to the Present. Within the late Pleistocene, large amplitude (1–6 g/cm^2/k.y.) variations in calcium carbonate accumulation can be resolved. These cycles are attributed to carbonate dissolution. Since this site is well above the regional lysocline, the cycles are presumed to reflect a shoaling of the local lysocline in an area influenced by high primary productivity in the surface waters. Therefore, these dissolution cycles may provide an indirect monitor of organic carbon flux to the sediments.

ACKNOWLEDGMENTS

This research was supported by grants from the National Science Foundation (OCE-8511571) and JOI/USSAC(TAMRF-20172). Dr. P. Froelich and R. Mortlock (LDGO) kindly provided us with laboratory supplies and machine time for the RC27-61 opal measurements. We gratefully acknowledge S. Balakrishnan (C-org), J. Harrigan ($CaCO_3$; coarse fraction), T. Saha (coarse fraction); E. Grossman ($CaCO_3$); D. Verardo (LDGO-opal); and A. deCharon (opal) for their technical help.

REFERENCES

Clemens, S. C., and Prell, W. L., 1990. Late Pleistocene variability of Arabian Sea summer-monsoon winds and dust source-area aridity: eolian records from the lithogenic component of deep-sea sediments. *Paleoceanography*, 5:109–145.

Cullen, J., and Prell, W. L., 1984. Planktonic foraminifera of the northern Indian Ocean: distribution and preservation in surface sediments. *Mar. Micropaleontol.*, 9:1–52.

Fischer, K., Dymond, J., Lyle, M., Soutar, A., and Rau, S., 1986. The benthic cycle of copper: evidence from sediment trap experiments in the eastern tropical North Pacific Ocean. *Geochim. Cosmochim. Acta*, 50:1535–1543.

Imbrie, J., Hays, J. D., Martinson, D. G., McIntyre, A., Mix, A. C., Morley, J. J., Pisias, N. G., Prell, W. L., and Shackleton, N. J., 1984. The orbital theory of Pleistocene climate: support from a revised chronology of the marine delta $\delta^{18}O$ record. *In* Berger, A., Imbrie, J., Hays, J., Kukla, G., and Saltzman, B. (Eds.), *Milankovitch and Climate* (Pt. 1): Dordrecht (D. Reidel), 269–305.

Jenkins, G. M., and Watts, D. G., 1968. *Spectral Analysis and its Applications*: Oakland (Holden Day).

Jones, G. A., and Kaiteris, P., 1983. A vacuum-gasometric technique for rapid and precise analysis of calcium carbonate in sediments and soils. *J. Sediment. Petrol.*, 53:655–660.

Kutzbach, J. E., and Guetter, P. J., 1986. The influence of changing orbital parameters and surface boundary conditions on climate simulations for the past 18,000 years. *J. Atmos. Sci.*, 43:1726–1759.

Mortlock, R. A., and Froelich, P. N., 1989. A simple method for the rapid determination of biogenic opal in pelagic marine sediments. *Deep-Sea Res. Part A*, 36:1415–1426.

Müller, P. J., and Suess, E., 1979. Productivity, sedimentation rate, and sedimentary organic matter in the oceans. I. Organic carbon preservation. *Deep-Sea Res. Part A*, 26:1347–1362.

Peterson, L. C., and Prell, W. L., 1985. Carbonate preservation and rates of climatic change: an 800 kyr record from the Indian Ocean. *In* Sundquist, E. T., and Broecker, W. S. (Eds.), *The Carbon Cycle and Atmospheric CO_2: Natural Variations Archean to Present*: Am. Geophys. Union Monogr., 32:251–270.

Prell, W. L., 1984a. Monsoonal climate of the Arabian Sea during the late Quaternary: a response to changing solar radiation. *In* Berger, A. L., Imbrie, J., Hays, J., Kukla, G., and Saltzman, B. (Eds.). *Milankovitch and Climate* (Pt. 1): Dordrecht (D. Reidel), 349–366.

_____, 1984b. Variation of monsoonal upwelling: a response to changing solar radiation. *In* Hansen, J. E., and Takahashi, T. (Eds.), *Climatic Processes and Climate Sensitivity.* Am. Geophys. Union, Maurice Ewing Ser., 29:48–57.

Prell, W. L., and Kutzbach, J. E., 1987. Monsoon variability over the past 150,000 years. *J. Geophys. Res.*, 92:8411–8425.

Prell, W. L., Niitsuma, N., et al., 1989. *Proc. ODP, Init. Repts.*, 117: College Station, TX (Ocean Drilling Program).

Prell, W. L., and Van Campo, E., 1986. Coherent response of Arabian Sea upwelling and pollen transport to late Quaternary monsoonal winds. *Nature*, 323:526–528.

Raymo, M. E., Ruddiman, W. F., Backman, J., Clement, B. M., and Martinson, D. G., 1989. Late Pliocene variation in Northern Hemisphere ice sheets and North Atlantic Deep Water circulation. *Paleoceanography*, 4:413–446.

Ruddiman, W. F., Raymo, M. E., Martinson, D. G., Clement, B. M., and Backman, J., 1989. Pleistocene evolution: Northern Hemisphere ice sheets and North Atlantic Ocean. *Paleoceanography*, 4:353–412.

Sarnthein, M., and Winn, K., Duplessy, J.-C., Fontugne, M. R., 1988. Global variations of surface ocean productivity in low and mid latitudes: influence on CO_2 reservoirs of the deep ocean and atmosphere during the last 21,000 years. *Paleoceanography*, 3:361–399.

Shipboard Scientific Party, 1989. Site 722. *In* Prell, W. L., Niitsuma, N., et al., *Proc. ODP, Init. Repts.*, 117: College Station, TX (Ocean Drilling Program), 255–318.

Sirocko, F., and Sarnthein, M., 1989. Wind-borne deposits in the northwest Indian Ocean: record of Holocene sediments versus modern satellite data. *In* Leinen, M., and Sarnthein, M. (Eds.), *Paleoclimatology and Paleometeorology: Modern and Past Patterns of Global Atmospheric Transport.* NATO ASI Ser., 282:401–433.

Verardo, D., Froelich, P. N., McIntrye, A., 1990. Determination of organic carbon and nitrogen in marine sediments using the Carlo Erba NA-1500 Analyzer, *Deep-Sea Res. Part A*, 37:157–165.

Date of initial receipt: 28 September 1989
Date of acceptance: 25 July 1990
Ms 117B-141

APPENDIX
Hole 722B Composite

Core, section	Section depth (cm)	ODP depth (m)	Composite[a] depth (m)	Ship[b] age (m.y.)	Ship sed. rate (cm/k.y.)	Isotope[c] age (m.y.)	Isotope sed. rate (cm/k.y.)	Composite[d] susceptibility (10^{-6}cgs)	Composite[e] density (g/cm^3)	$CaCO_3$ (%)	Composite[f] $CaCO_3$ (%)	>150 μm (%)	C-org (%)	$\delta^{18}O$ (‰)
1H-1	1	0.01	0.01	0.0002	4.12	0.0060	8.47	[g]7.00	0.756	73.17	73.17	12.1	1.067	−1.470
1H-1	21	0.21	0.21	0.0051	4.12	0.0084	8.47	[g]3.64	0.812	78.05	78.05	22.4	0.748	−0.970
1H-1	41	0.41	0.41	0.0100	4.12	0.0107	8.47	[g]10.96	0.847	71.69	71.69	21.8	0.783	−0.225
1H-1	61	0.61	0.61	0.0148	4.12	0.0131	8.47	[g]21.52	0.928	66.30	66.30	11.9	0.745	0.170
1H-1	81	0.81	0.81	0.0197	4.12	0.0154	8.47	[g]13.98	0.931	65.46	65.46	14.7	0.912	0.170
1H-1	101	1.01	1.01	0.0245	4.12	0.0178	6.19	[g]13.98	0.927	63.15	63.15	12.9	1.091	0.430
1H-1	121	1.21	1.21	0.0294	4.12	0.0219	4.87	[g]15.84	0.981	61.95	61.95	12.0	0.882	0.200
1H-1	141	1.41	1.41	0.0343	4.12	0.0260	4.87	[g]10.60	0.895	64.15	64.15	18.9	1.110	0.490
1H-2	11	1.61	1.61	0.0391	4.12	0.0301	4.87	[g]15.08	0.918	61.66	61.66	12.5	0.911	0.230
1H-2	31	1.81	1.81	0.0440	4.12	0.0342	4.87	[g]12.58	0.998	62.11	62.11	15.0	1.027	−0.060
1H-2	51	2.01	2.01	0.0488	4.12	0.0383	4.87	[g]9.42	0.908	68.06	68.06	17.5	1.120	−0.080
1H-2	71	2.21	2.21	0.0537	4.12	0.0424	4.87	[g]6.52	0.845	65.51	65.51	13.8	1.111	−0.010
1H-2	91	2.41	2.41	0.0585	4.12	0.0465	4.88	[g]6.02	0.919	60.84	60.84	10.2	1.054	−0.220
1H-2	111	2.61	2.61	0.0634	4.12	0.0506	4.87	[g]3.38	0.862	71.13	71.13	9.9	1.122	−0.440
1H-2	131	2.81	2.81	0.0683	4.12	0.0547	4.87	[g]5.40	0.907	69.17	69.17	8.8	0.879	0.030
1H-3	1	3.01	3.01	0.0731	4.12	0.0588	4.87	[g]9.44	0.842	64.87	64.87	12.8	0.790	−0.300
1H-3	21	3.21	3.21	0.0780	4.12	0.0630	4.37	[g]19.76	1.050	58.55	58.55	8.8	0.625	0.190
1H-3	41	3.41	3.41	0.0828	4.12	0.0680	3.62	[g]15.12	1.021	59.80	59.80	7.3	0.746	0.150
1H-3	61	3.61	3.61	0.0877	4.12	0.0740	3.33	[g]9.80	1.042	61.05	61.05	7.4	0.722	−0.370
1H-3	81	3.81	3.81	0.0925	4.12	0.0800	2.58	[g]5.68	0.877	67.18	67.18	11.7	0.566	−0.530
1H-3	101	4.01	4.01	0.0974	4.10	0.0895	2.11	[g]5.96	0.970	64.07	64.07	17.1	0.531	−0.410
1H-3	121	4.21	4.21	0.1023	4.12	0.0990	2.14	[g]3.38	0.850	72.30	72.30		0.719	−0.985
1H-3	141	4.41	4.41	0.1071	4.12	0.1082	2.17	[g]4.34	1.012	70.32	70.32	11.2	0.758	−0.510
1H-4	11	4.61	4.61	0.1120	4.12	0.1174	2.60	[g]7.16	[h]0.958	68.22	68.22	3.7	0.660	−1.160
1H-4	31	4.81	4.81	0.1168	4.12	0.1236	4.30	[g]3.64	[h]0.897	78.13	78.13	17.3	0.655	−1.110
1H-4	51	5.01	5.01	0.1217	4.12	0.1267	6.45	[g]13.00	[h]0.985	64.13	64.13	8.3	0.396	−0.195
1H-4	71	5.21	5.21	0.1265	4.11	0.1298	6.39	[g]10.22	[h]0.965	64.12	64.12	8.9	0.644	0.260
2H-1	4	5.54	5.54	0.1346	4.10	0.1350	6.10	[g, h]10.33	[h]0.978	65.52	[i]68.14	10.8	1.139	0.430
2H-1	21	5.71	5.71	0.1387	4.16	0.1380	5.78	[g]6.62	0.887	62.90	62.90	16.6	0.951	0.050
2H-1	41	5.91	5.91	0.1435	4.12	0.1414	5.80	[g]8.86	1.032	65.26	65.26	15.3	0.670	0.160
2H-1	61	6.11	6.11	0.1484	4.08	0.1449	5.71	[g]13.14	0.989	62.95	62.95	14.2	0.627	0.200
2H-1	81	6.31	6.31	0.1533	4.12	0.1484	5.71	[g]21.70	1.132	57.80	57.80	12.5	0.747	−0.010
2H-1	101	6.51	6.51	0.1581	4.12	0.1519	5.80	[g]12.34	1.036	59.42	59.42	14.3	0.808	0.150
2H-1	121	6.71	6.71	0.1630	4.12	0.1553	5.80	8.42	1.081	52.57	52.57	8.9	0.900	−0.120
2H-1	141	6.91	6.91	0.1678	4.12	0.1588	5.71	7.22	0.996	53.04	53.04	9.4	0.832	0.020
2H-2	11	7.11	7.11	0.1727	4.12	0.1623	5.71	5.26	0.940	58.91	58.91	11.8	0.797	0.020
2H-2	31	7.31	7.31	0.1775	4.12	0.1658	5.71	4.30	0.958	63.55	63.55	15.7	0.821	−0.270
2H-2	51	7.51	7.51	0.1824	4.08	0.1693	5.26	5.44	1.043	57.47	57.47	8.6	0.486	−0.360
2H-2	71	7.71	7.71	0.1873	4.12	0.1734	4.49	4.34	0.958	63.22	63.22	19.3	0.631	−0.395
2H-2	91	7.91	7.91	0.1921	4.12	0.1782	4.17	4.52	1.025	60.82	60.82	6.4	0.753	−0.140
2H-2	111	8.11	8.11	0.1970	4.12	0.1830	2.94	3.94	1.043	60.69	60.69	7.1	0.750	0.020
2H-2	131	8.31	8.31	0.2018	4.12	0.1918	2.26	1.06	0.978	80.02	80.02	10.4	0.522	−0.785
2H-3	1	8.51	8.51	0.2067	4.12	0.2007	2.25	1.78	0.971	76.83	76.83	13.4	0.613	−0.820
2H-3	21	8.71	8.71	0.2115	4.12	0.2096	2.26	2.46	0.842	73.01	73.01	10.6	0.543	−1.170
2H-3	41	8.91	8.91	0.2164	4.08	0.2184	3.15	1.28	0.876	76.73	76.73	11.1	0.670	−0.720
2H-3	61	9.11	9.11	0.2213	4.12	0.2223	5.13	2.18	0.963	65.27	65.27	9.3	0.416	−0.830
2H-3	81	9.31	9.31	0.2261	4.12	0.2262	5.06	5.16	1.108	58.12	58.12	8.1	0.645	−0.265
2H-3	101	9.51	9.51	0.2310	4.12	0.2302	5.06	3.38	1.025	68.15	68.15	7.6	0.942	−0.480
2H-3	121	9.71	9.71	0.2358	4.12	0.2341	5.13	4.04	1.000	68.36	68.36	5.2	0.760	−0.360
2H-3	141	9.91	9.91	0.2407	4.12	0.2380	5.26	2.32	1.009	74.14	74.14	5.7	0.755	−0.790
2H-4	11	10.11	10.11	0.2455	4.12	0.2417	5.48	4.02	0.982	65.79	65.79	13.8	0.401	−0.370
2H-4	31	10.31	10.31	0.2504	4.08	0.2453	5.48	3.86	0.982	64.62	64.62	13.2	0.816	−0.110
2H-4	51	10.51	10.51	0.2553	4.12	0.2490	5.71	3.56	0.922	68.27	68.27	17.1	1.149	−0.010
2H-4	71	10.71	10.71	0.2601	4.12	0.2523	5.97	2.74	0.931	68.28	68.28	15.2	0.966	−0.030
2H-4	91	10.91	10.91	0.2650	4.12	0.2557	5.97	2.50	0.841	63.98	63.98	14.5	0.845	−0.080
2H-4	111	11.1	11.11	0.2698	4.12	0.2590	6.06	2.88	0.889	64.05	64.05	11.5	0.743	0.070
2H-4	131	11.31	11.31	0.2747	4.12	0.2623	5.97	4.42	1.038	57.40	57.40	5.3	0.485	0.070
2H-5	1	11.51	11.51	0.2795	4.12	0.2657	5.97	4.98	1.118	56.28	56.28	7.1	0.470	0.310
2H-5	21	11.71	11.71	0.2844	4.08	0.2690	3.25	5.36	1.073	58.82	58.82	6.5	0.524	0.340
2H-5	41	11.91	11.91	0.2893	4.12	0.2780	2.22	3.88	1.038	63.69	63.69	4.2	0.783	−0.290
2H-5	61	12.11	12.11	0.2941	4.12	0.2870	2.67	1.62	1.021	75.96	75.96	7.5	0.579	−0.570
2H-5	81	12.31	12.31	0.2990	4.12	0.2930	3.33	2.14	1.005	72.84	72.84	4.9	0.582	−0.290
2H-5	101	12.51	12.51	0.3038	4.12	0.2990	2.86	2.28	1.040	70.69	70.69	4.3	0.812	−0.170
2H-5	121	12.71	12.71	0.3087	4.08	0.3070	2.50	1.70	0.934	71.26	71.26	4.2	0.552	−0.385
2H-5	141	12.91	12.91	0.3136	4.12	0.3150	2.50	0.68	0.954	80.92	80.92	8.8	0.594	−0.765
2H-6	11	13.11	13.11	0.3184	4.12	0.3230	2.50	2.32	0.980	78.53	78.53	4.5	0.579	−0.680
2H-6	31	13.31	13.31	0.3233	4.12	0.3310	3.67	1.82	0.904	79.94	79.94	6.5	0.666	−1.180
2H-6	51	13.51	13.51	0.3281	4.12	0.3339	7.02	1.86	0.967	82.53	82.53	9.4	0.610	−0.750
2H-6	71	13.71	13.71	0.3330	4.12	0.3367	7.02	2.76	1.036	77.67	77.67	6.3	0.523	−0.350
2H-6	91	13.91	13.91	0.3378	4.12	0.3396	6.25	3.22	1.066	71.58	71.58	5.5	0.624	0.110
2H-6	111	14.11	14.11	0.3427	4.08	0.3431	5.13	3.14	0.981	71.24	71.24	7.2	0.802	[j]0.360
2H-6	131	14.31	14.31	0.3476	4.12	0.3474	4.71	3.18	1.011	72.08	72.08	8.5	0.975	0.060
2H-7	1	14.51	14.51	0.3524	4.12	0.3516	4.71	3.22	[h]1.019	70.78	70.78	9.0	0.863	−0.050
2H-7	21	14.71	14.71	0.3573	4.11	0.3559	4.69	[h]3.32	[h]1.019	70.47	70.47	9.1	0.719	−0.270

Appendix (continued).

Core, section	Section depth (cm)	ODP depth (m)	Composite[a] depth (m)	Ship[b] age (m.y.)	Ship sed. rate (cm/k.y.)	Isotope[c] age (m.y.)	Isotope sed. rate (cm/k.y.)	Composite[d] susceptibility (10^{-6}cgs)	Composite[e] density (g/cm^3)	$CaCO_3$ (%)	Composite[f] $CaCO_3$ (%)	>150 μm (%)	C-org (%)	$\delta^{18}O$ (‰)
3H-1	1	15.11	15.11	0.3670	4.14	0.3644	4.72	[h]2.44	[h]1.073	73.69	73.69	5.8	0.852	−0.385
3H-1	21	15.31	15.31	0.3718	4.13	0.3686	4.72	[h]2.96	0.920	72.74	72.74	5.4	0.906	−0.320
3H-1	41	15.51	15.61	0.3791	4.10	0.3750	4.03	2.64	0.878	74.18	74.18	4.7	0.849	−0.220
3H-1	61	15.71	15.81	0.3840	4.12	0.3810	3.33	1.70	0.997	80.96	80.96	4.7	0.865	−0.360
3H-1	81	15.91	16.01	0.3888	4.12	0.3870	3.33	2.06	0.924	78.06	78.06	3.7	0.590	−0.780
3H-1	101	16.11	16.21	0.3937	4.08	0.3930	3.33	2.74	0.986	74.38	74.38	3.7	1.086	−0.520
3H-1	121	16.31	16.41	0.3986	4.12	0.3990	3.33	1.06	0.996	82.16	82.16	2.4	0.777	−1.210
3H-1	141	16.51	16.61	0.4034	4.12	0.4050	1.67	0.94	1.000	83.07	83.07	4.9	0.692	−1.310
3H-2	11	16.71	16.81	0.4083	4.12	0.4230	1.84	1.52	0.919	80.60	80.60	5.4	0.879	−0.400
3H-2	31	16.91	17.01	0.4131	4.12	0.4267	5.48	2.80	1.023	73.17	73.17	4.0	1.133	−0.010
3H-2	51	17.11	17.21	0.4180	4.12	0.4303	5.48	4.84	1.039	66.96	66.96	7.5	0.865	0.410
3H-2	71	17.31	17.41	0.4228	4.12	0.4340	4.88	4.02	1.021	68.80	68.80	6.3	1.083	0.460
3H-2	91	17.51	17.61	0.4277	4.08	0.4385	4.44	3.08	0.989	71.09	71.09	7.8	1.191	0.310
3H-2	111	17.71	17.81	0.4326	4.12	0.4430	4.44	4.30	1.083	65.24	65.24	7.0	0.865	[j]0.430
3H-2	131	17.91	18.01	0.4374	4.12	0.4475	4.44	2.96	0.935	67.88	67.88	7.9	0.942	0.320
3H-3	1	18.11	18.21	0.4423	4.12	0.4520	4.44	2.76	0.939	74.10	74.10	13.0	1.159	0.170
3H-3	21	18.31	18.41	0.4471	4.12	0.4565	4.44	2.68	0.870	72.75	72.75	12.5	1.261	−0.030
3H-3	41	18.51	18.61	0.4520	4.12	0.4610	4.21	3.20	0.958	72.71	72.71	6.5	0.775	−0.120
3H-3	61	18.71	18.81	0.4568	4.12	0.4660	4.00	3.60	0.930	67.13	67.13	14.6	1.734	−0.020
3H-3	81	18.91	19.01	0.4617	4.08	0.4710	3.42	2.58	0.940	71.31	71.31	5.6	1.330	0.090
3H-3	101	19.11	19.21	0.4666	4.12	0.4777	3.01	2.64	0.942	72.34	72.34	6.0	1.014	0.030
3H-3	121	19.31	19.41	0.4714	4.12	0.4843	3.01	2.66	1.017	73.07	73.07	11.6	1.439	−0.210
3H-3	141	19.51	19.61	0.4763	4.12	0.4910	2.26	2.18	0.992	71.83	71.83	8.1	1.194	−0.330
3H-4	11	19.71	19.81	0.4811	4.12	0.5020	1.82	2.96	0.974	74.75	74.75	4.5	0.622	−0.220
3H-4	31	19.91	20.01	0.4860	4.08	0.5130	2.60	4.38	1.069	68.60	68.60	4.0	0.777	−0.160
3H-4	51	20.11	20.21	0.4909	4.12	0.5174	4.55	3.30	1.019	70.03	70.03	2.5	0.873	−0.370
3H-4	71	20.31	20.41	0.4957	4.12	0.5218	3.54	2.92	1.008	70.65	70.65	5.2	1.165	−0.660
3H-4	91	20.51	20.61	0.5006	4.12	0.5287	2.47	2.84	1.086	71.50	71.50	5.4	0.910	−0.680
3H-4	111	20.71	20.81	0.5054	4.12	0.5380	1.72	2.40	1.042	71.07	71.07	11.5	0.955	−0.260
3H-4	131	20.91	21.01	0.5103	4.12	0.5520	1.60	3.36	1.073	71.65	71.65	9.1	1.011	−0.530
3H-5	1	21.11	21.21	0.5151	4.12	0.5630	1.82	3.44	1.000	70.85	70.85	10.7	0.860	−0.340
3H-5	21	21.31	21.41	0.5200	4.08	0.5740	1.82	4.32	1.029	71.44	71.44	4.9	0.789	−0.590
3H-5	41	21.51	21.61	0.5249	4.12	0.5850	1.82	4.10	1.047	69.25	69.25	5.3	0.840	[j]−0.410
3H-5	61	21.71	21.81	0.5297	4.12	0.5960	2.47	2.22	1.002	82.09	82.09	8.1	0.795	−1.450
3H-5	81	21.91	22.01	0.5346	4.12	0.6012	3.81	3.98	1.066	70.45	70.45	6.6	0.729	−0.610
3H-5	101	22.11	22.21	0.5394	4.12	0.6065	3.81	3.74	0.957	71.59	71.59	3.1	0.946	−0.370
3H-5	121	22.31	22.41	0.5443	4.12	0.6117	3.81	3.46	0.934	69.88	69.88	7.4	0.858	−0.420
3H-5	141	22.51	22.61	0.5491	4.12	0.6170	3.70	2.82	1.079	75.87	75.87	4.9	1.141	−0.760
3H-6	11	22.71	22.81	0.5540	4.08	0.6225	3.64	3.76	0.970	75.30	75.30	15.1	0.937	−0.490
3H-6	31	22.91	23.01	0.5589	4.12	0.6280	4.21	5.28	1.024	61.54	61.54	13.6	1.418	0.480
3H-6	51	23.11	23.21	0.5637	4.12	0.6320	5.00	4.92	1.070	64.93	64.93	18.4	1.486	0.320
3H-6	71	23.31	23.41	0.5686	4.12	0.6360	5.00	4.60	1.029	65.36	65.36	13.4	1.425	0.300
3H-6	91	23.51	23.61	0.5734	4.12	0.6400	5.00	4.68	1.077	64.46	64.46	15.8	1.084	0.245
3H-6	111	23.71	23.81	0.5783	4.12	0.6440	5.00	4.58	1.012	68.43	68.43	17.0	1.013	−0.020
3H-6	131	23.91	24.01	0.5831	4.12	0.6480	5.00	4.62	1.059	67.96	67.96	14.6	1.493	0.030
3H-7	1	24.11	24.21	0.5880	4.08	0.6520	5.00	4.90	1.095	66.58	66.58	16.0	1.539	0.060
3H-7	21	24.31	24.41	0.5929	4.12	0.6560	4.12	5.74	1.043	60.95	60.95	9.8	1.127	0.105
3H-7	41	24.51	24.61	0.5977	4.12	0.6617	3.48	5.08	0.970	65.58	65.58	11.5	1.385	−0.220
3H-7	61	24.71	24.81	0.6026	4.12	0.6675	3.47	[k]4.58	0.967	64.90	64.90	9.9	1.052	−0.105
4H-1	1	24.71	24.96	0.6062	4.12	0.6718	3.50	[k]4.24	0.967	64.88	64.88	7.6	0.827	−0.210
4H-1	21	24.91	25.16	0.6111	4.12	0.6775	3.48	[k]4.12	0.967	69.90	[l]64.80	6.9	1.120	−0.240
4H-1	41	25.11	25.36	0.6159	4.12	0.6833	3.48	[k]1.92	0.787	68.68	68.68	7.3	1.143	−0.620
4H-1	61	25.31	25.56	0.6208	4.12	0.6890	4.26	[k]1.48	0.779	64.80	[l]69.90	11.4	1.487	−0.865
4H-1	81	25.51	25.76	0.6256	4.12	0.6927	5.48	[k]1.92	0.911	68.59	68.59	15.8	1.726	−0.380
4H-1	101	25.71	25.96	0.6305	4.08	0.6963	5.48	4.46	1.132	60.92	60.92	6.7	0.693	0.160
4H-1	121	25.91	26.16	0.6354	4.12	0.7000	5.56	5.72	1.124	55.18	55.18	6.3	0.722	0.050
4H-1	141	26.11	26.36	0.6402	4.12	0.7035	5.71	3.50	1.131	62.24	62.24	9.0	1.171	0.180
4H-2	11	26.31	26.56	0.6451	4.12	0.7070	5.71	2.64	0.928	70.82	70.82	7.0	1.404	−0.210
4H-2	31	26.51	26.76	0.6499	4.12	0.7105	5.71	1.82	1.000	73.78	73.78	13.2	1.282	−0.030
4H-2	51	26.71	26.96	0.6548	4.12	0.7140	5.71	1.64	0.873	71.95	71.95	11.9	1.435	−0.430
4H-2	71	26.91	27.16	0.6596	4.12	0.7175	5.71	4.00	0.986	64.49	64.49	13.8	0.657	0.100
4H-2	91	27.11	27.36	0.6645	4.08	0.7210	6.25	1.76	0.930	73.47	73.47	16.0	1.268	−0.250
4H-2	111	27.31	27.56	0.6694	4.12	0.7239	7.02	1.86	0.911	72.15	72.15	12.5	1.300	−0.060
4H-2	131	27.51	27.76	0.6742	4.12	0.7267	7.02	2.10	0.938	71.72	71.72	7.8	0.859	−0.400
4H-3	1	27.71	27.96	0.6791	4.12	0.7296	5.63	2.52	1.036	67.02	67.02	6.1	0.742	−0.540
4H-3	21	27.91	28.16	0.6839	4.12	0.7338	4.12	2.70	0.971	66.08	66.08	4.8	0.945	−0.510
4H-3	41	28.11	28.36	0.6888	4.08	0.7393	3.60	2.72	1.021	70.02	70.02	13.3	1.047	−0.280
4H-3	61	28.31	28.56	0.6937	4.12	0.7449	3.60	4.90	1.081	62.81	62.81	10.5	0.886	−0.030
4H-3	81	28.51	28.76	0.6985	4.12	0.7504	3.60	4.64	1.086	62.98	62.98	8.6	0.890	0.000
4H-3	101	28.71	28.96	0.7034	4.12	0.7560	4.44	4.12	1.015	65.85	65.85	12.8	0.945	0.110
4H-3	121	28.91	29.16	0.7082	4.12	0.7594	5.88	3.96	0.882	61.80	61.80	8.2	1.161	0.010
4H-3	141	29.11	29.36	0.7131	4.12	0.7628	5.80	2.72	1.059	67.98	67.98	4.6	1.188	−0.535
4H-4	11	29.31	29.56	0.7179	4.12	0.7663	5.80	2.42	0.908	71.11	71.11	3.8	1.341	−0.520
4H-4	31	29.51	29.76	0.7228	4.08	0.7697	5.88	2.04	0.970	75.91	75.91	5.5	0.954	−0.610
4H-4	51	29.71	29.96	0.7277	4.12	0.7731	5.88	1.72	0.904	74.51	74.51	3.8	1.335	−0.880
4H-4	71	29.91	30.16	0.7325	4.12	0.7765	5.88	2.68	0.982	69.79	69.79	7.3	0.993	−0.470

Appendix (continued).

Core, section	Section depth (cm)	ODP depth (m)	Composite[a] depth (m)	Ship[b] age (m.y.)	Ship sed. rate (cm/k.y.)	Isotope[c] age (m.y.)	Isotope sed. rate (cm/k.y.)	Composite[d] susceptibility (10^{-6}cgs)	Composite[e] density (g/cm^3)	$CaCO_3$ (%)	Composite[f] $CaCO_3$ (%)	>150 μm (%)	C-org (%)	$\delta^{18}O$ (‰)
4H-4	91	30.11	30.36	0.7374	4.12	0.7799	5.88	1.64	0.885	77.40	77.40	6.9	1.208	−0.970
4H-4	111	30.31	30.56	0.7422	4.12	0.7833	5.88	2.40	1.043	75.32	75.32	8.8	0.920	−0.940
4H-4	131	30.51	30.76	0.7471	4.12	0.7867	5.80	2.06	0.916	71.80	71.80	5.1	1.176	−0.870
4H-5	1	30.71	30.96	0.7519	4.12	0.7902	5.80	2.92	0.989	76.21	76.21	10.0	1.403	−0.300
4H-5	21	30.91	31.16	0.7568	4.08	0.7936	5.88	5.36	1.023	64.47	64.47	8.3	0.614	0.130
4H-5	41	31.11	31.36	0.7617	4.12	0.7970	6.67	5.84	1.178	58.51	58.51	7.4	0.923	0.190
4H-5	61	31.31	31.56	0.7665	4.12	0.7996	7.84	5.50	0.997	55.44	55.44	9.3	1.984	0.180
4H-5	81	31.51	31.76	0.7714	4.12	0.8021	7.84	4.78	1.002	61.55	61.55	12.6	1.403	0.040
4H-5	101	31.71	31.96	0.7762	4.12	0.8047	7.69	5.16	1.086	61.75	61.75	6.3	1.139	0.130
4H-5	121	31.91	32.16	0.7811	4.12	0.8073	7.84	6.28	1.105	55.96	55.96	6.3	0.661	0.010
4H-5	141	32.11	32.36	0.7859	4.12	0.8098	7.84	6.42	1.164	56.87	56.87	5.4	0.775	0.030
4H-6	11	32.31	32.56	0.7908	4.08	0.8124	7.84	4.88	1.087	64.61	64.61	5.3	1.819	0.120
4H-6	31	32.51	32.76	0.7957	4.12	0.8149	7.84	2.42	0.896	67.37	67.37	8.6	1.664	−0.020
4H-6	51	32.71	32.96	0.8005	4.12	0.8175	2.90	3.16	1.025	69.47	69.47	8.0	1.836	−0.450
4H-6	71	32.91	33.16	0.8054	4.12	0.8287	1.79	5.04	0.927	64.90	64.90	9.7	1.692	−0.030
4H-6	91	33.11	33.36	0.8102	4.12	0.8399	2.63	7.38	1.168	54.53	54.53	5.7	0.891	0.210
4H-6	111	33.31	33.56	0.8151	4.12	0.8439	5.00	6.04	1.132	59.79	59.79	8.8	1.264	0.000
4H-6	131	33.51	33.76	0.8199	4.12	0.8479	5.00	6.34	1.042	58.03	58.03	4.8	0.980	−0.050
4H-7	1	33.71	33.96	0.8248	4.08	0.8519	5.00	5.80	1.166	61.34	61.34	4.7	0.689	−0.180
4H-7	21	33.91	34.16	0.8297	4.12	0.8559	5.00	5.82	[k]1.106	60.30	60.30	3.7	0.914	−0.440
4H-7	41	34.11	34.36	0.8345	4.12	0.8600	4.55	5.20	[k]1.093	64.45	64.45	3.3	1.050	−0.570
4H-7	61	34.31	34.56	0.8394	4.08	0.8647	3.88	5.50	[k]1.079	57.61	57.61	1.9	1.329	[j]−1.020
5H-1	1	34.31	34.56	0.8394	4.08	0.8647	3.88			59.98		2.8		−0.470
5H-1	21	34.51	34.76	0.8442	4.12	0.8703	3.60	3.46	0.884	59.96	59.96	6.3		−0.600
5H-1	41	34.71	34.96	0.8491	4.12	0.8758	3.60	5.00	1.027	55.59	55.59	3.4		−0.090
5H-1	61	34.91	35.16	0.8539	4.12	0.8814	4.65	5.46	1.089	63.47	63.47	6.2	0.810	−0.110
5H-1	81	35.11	35.36	0.8588	4.08	0.8844	6.67	3.88	1.086	68.60	68.60	2.0	1.082	−0.200
5H-1	101	35.31	35.56	0.8637	4.12	0.8874	6.56	3.54	1.031	65.71	65.71	3.3	1.322	−0.770
5H-1	121	35.51	35.76	0.8685	4.12	0.8905	6.56	3.08	1.012	68.07	68.07	5.7	0.979	−0.690
5H-1	141	35.71	35.96	0.8734	4.12	0.8935	6.67	2.70	0.985	72.87	72.87	6.8	0.734	−0.670
5H-2	11	35.91	36.16	0.8782	4.12	0.8965	6.67	3.14	0.950	72.16	72.16	2.2	1.130	−0.570
5H-2	31	36.11	36.36	0.8831	4.08	0.8995	5.06	3.88	1.031	66.04	66.04	2.1		−0.410
5H-2	51	36.31	36.56	0.8880	4.12	0.9044	4.08	2.66	0.994	70.01	70.01	2.7	1.330	
5H-2	71	36.51	36.76	0.8928	4.12	0.9093	4.08	0.86	0.943	80.56	80.56	9.5		−1.180
5H-2	91	36.71	36.96	0.8977	4.12	0.9142	4.08	3.80	0.982	66.35	66.35	5.8	0.839	−0.605
5H-2	111	36.91	37.16	0.9025	4.12	0.9191	3.60	4.08	1.046	67.78	67.78	3.4	1.093	−0.530
5H-2	131	37.11	37.36	0.9074	4.12	0.9253	2.92	2.90	1.062	70.99	70.99	4.7		−0.450
5H-3	1	37.31	37.56	0.9122	4.12	0.9328	2.67	4.28	0.981	62.50	62.50	7.9		−0.690
5H-3	21	37.51	37.76	0.9171	4.08	0.9403	2.67	3.58	0.994	68.09	68.09	9.8	0.722	−1.220
5H-3	41	37.71	37.96	0.9220	4.12	0.9478	2.86	3.38	0.961	67.18	67.18	9.9	0.968	[j]−0.820
5H-3	61	37.91	38.16	0.9268	4.12	0.9543	3.08	3.22	0.994	67.71	67.71	7.3	1.485	−1.110
5H-3	81	38.11	38.36	0.9317	4.12	0.9608	3.08	2.44	0.904	67.66	67.66	11.6	1.172	−0.640
5H-3	101	38.31	38.56	0.9365	4.12	0.9673	3.25	4.58	1.048	60.92	60.92	9.6	0.936	−0.690
5H-3	121	38.51	38.76	0.9414	4.12	0.9731	3.67	5.52	1.122	58.27	58.27	7.4	0.791	−0.860
5H-3	141	38.71	38.96	0.9462	4.12	0.9782	3.92	6.82	1.109	54.72	54.72	2.6	0.681	−0.630
5H-4	11	38.91	39.16	0.9511	4.08	0.9833	3.92	4.14	0.943	61.53	61.53	6.4	0.911	
5H-4	31	39.11	39.36	0.9560	4.12	0.9884	5.48	2.50	0.959	74.59	74.59	13.0	1.036	−1.320
5H-4	51	39.31	39.56	0.9608	4.12	0.9906	8.89	3.32	0.904	63.99	63.99	9.7	0.830	−0.770
5H-4	71	39.51	39.76	0.9657	4.12	0.9929	8.89	2.94	0.924	70.82	70.82	14.6	0.886	−0.630
5H-4	91	39.71	39.96	0.9705	4.12	0.9951	9.09	4.90	1.066	63.95	63.95	7.8		−0.400
5H-4	111	39.91	40.16	0.9754	4.08	0.9973	9.09	4.48	1.039	66.20	66.20	8.2	0.753	−0.400
5H-4	131	40.11	40.36	0.9803	3.64	0.9995	8.51	2.82	0.944	73.43	73.43	17.4	1.247	−0.480
5H-5	1	40.31	40.56	0.9864	3.28	1.0020	8.89	4.30	1.020	62.99	62.99	19.3	1.373	−0.280
5H-5	21	40.51	40.76	0.9925	3.31	1.0040	10.00	6.28	1.100	54.64	54.64	10.4	1.001	−0.050
5H-5	41	40.71	40.96	0.9985	3.20			5.72	1.039	60.86	60.86	11.5	0.953	−0.200
5H-5	61	40.91	41.16	1.0050	3.20			6.10	1.086	56.92	56.92	7.4	0.707	−0.360
5H-5	81	41.11	41.36	1.0110	3.33			4.48	1.079	66.52	66.52	6.6	0.774	−0.720
5H-5	101	41.31	41.56	1.0170	3.33			3.34	1.039	73.46	73.46	8.5	0.735	−0.660
5H-5	121	41.51	41.76	1.0230	3.33			3.62	1.044	69.28	69.28	4.1	0.880	−0.640
5H-5	141	41.71	41.96	1.0290	3.33			2.88	1.032	69.68	69.68	6.6	0.907	−1.100
5H-6	11	41.91	42.16	1.0350	3.33			3.10	0.982	72.96	72.96	9.5	0.889	−0.690
5H-6	31	42.11	42.36	1.0410	3.33			3.24	0.970	67.68	67.68	9.3	1.188	−0.380
5H-6	51	42.31	42.56	1.0470	3.33			2.28	0.950	73.94	73.94	15.3	0.912	−0.960
5H-6	71	42.51	42.76	1.0530	3.33			3.54	0.986	70.36	70.36	14.4	1.178	−0.300
5H-6	91	42.71	42.96	1.0590	3.33			3.58	1.023	65.64	65.64	12.5	1.047	−0.190
5H-6	111	42.91	43.16	1.0650	3.33			3.26	1.064	68.43	68.43	8.8	0.972	−0.630
5H-6	131	43.11	43.36	1.0710	3.08			3.68	1.032	67.70	67.70	12.1	0.960	−0.510
5H-7	1	43.31	43.56	1.0780	3.08			3.90	[k]1.073	68.98	68.98	7.8	1.183	−0.370
5H-7	21	43.51	43.76	1.0840	3.33			4.72	[k]1.006	63.30	63.30	8.8	0.821	−0.370
5H-7	41	43.71	43.96	1.0900	3.46			2.02	[k]1.059	78.67	78.67	6.9	1.034	−0.830
			44.21	1.0970	3.46			[k]1.66	[k]0.985		[i]78.78			
			44.41	1.1030	3.33			[k]2.50	[k]0.958		[i]73.92			
			44.61	1.1090	3.33			[k]3.46	[k]1.113		[i]68.35			
			44.81	1.1150	3.08			[k]5.78	[k]1.140		[i]54.91			
6H-1	1	43.91	45.01	1.1220	3.08			[k]5.58	[k]1.147	56.67	56.67	10.0	0.920	−0.170
6H-1	21	44.11	45.21	1.1280	3.33			4.90	1.069	60.79	60.79	8.3	1.045	−0.390

Appendix (continued).

Core, section	Section depth (cm)	ODP depth (m)	Composite[a] depth (m)	Ship[b] age (m.y.)	Ship sed. rate (cm/k.y.)	Isotope[c] age (m.y.)	Isotope sed. rate (cm/k.y.)	Composite[d] susceptibility (10^{-6}cgs)	Composite[e] density (g/cm^3)	$CaCO_3$ (%)	Composite[f] $CaCO_3$ (%)	>150 μm (%)	C-org (%)	$\delta^{18}O$ (‰)
6H-1	41	44.31	45.41	1.1340	3.33			5.18	1.031	62.96	62.96	7.1	0.721	−0.490
6H-1	61	44.51	45.61	1.1400	3.33			4.76	1.070	60.96	60.96	3.5	1.276	−0.340
6H-1	81	44.71	45.81	1.1460	3.33			2.72	1.012	72.88	72.88	9.9	1.602	−0.490
6H-1	101	44.91	46.01	1.1520	3.33			3.72	0.997	63.38	63.38	11.3	1.054	−0.640
6H-1	121	45.11	46.21	1.1580	3.33			4.92	1.012	56.44	56.44	8.3	1.288	−0.360
6H-1	141	45.31	46.41	1.1640	3.33			5.20	1.050	57.42	57.42	9.8	0.802	[j]−0.020
6H-2	11	45.51	46.61	1.1700	3.33			4.66	1.021	59.94	59.94	9.6	0.725	−0.270
6H-2	31	45.71	46.81	1.1760	3.33			5.78	1.048	54.90	54.90	3.7	0.636	−0.450
6H-2	51	45.91	47.01	1.1820	3.33			4.24	0.994	60.67	60.67	5.0	0.715	−0.660
6H-2	71	46.11	47.21	1.1880	3.33			1.98	0.998	74.98	74.98	11.9	0.863	−0.900
6H-2	91	46.31	47.41	1.1940	3.08			3.04	0.984	66.40	66.40	4.8	0.704	−0.730
6H-2	111	46.51	47.61	1.2010	3.08			4.64	0.998	53.75	53.75	3.7	0.800	−0.730
6H-2	131	46.71	47.81	1.2070	3.33			5.22	1.059	56.73	56.73	8.0	0.793	−0.540
6H-3	1	46.91	48.01	1.2130	3.33			4.78	1.097	58.44	58.44	7.6	0.879	−0.690
6H-3	21	47.11	48.21	1.2190	3.33			6.80	1.122	53.14	53.14	2.9	0.818	−0.490
6H-3	41	47.31	48.41	1.2250	3.33			2.18	0.986	77.30	77.30	6.4	0.526	−1.470
6H-3	61	47.51	48.61	1.2310	3.33			2.62	1.001	71.22	71.22	8.6	0.758	−1.020
6H-3	81	47.71	48.81	1.2370	3.33			2.40	0.971	69.98	69.98	7.1	1.072	−0.630
6H-3	101	47.91	49.01	1.2430	3.33			1.96	0.888	63.84	63.84	8.8	1.120	−0.830
6H-3	121	48.11	49.21	1.2490	3.33			3.52	0.908	71.65	71.65	14.1	1.090	−0.490
6H-3	141	48.31	49.41	1.2550	3.33			4.36	1.036	61.23	61.23	5.7	1.259	−0.410
6H-4	11	48.51	49.61	1.2610	3.33			2.76	0.967	68.43	68.43	7.1	1.195	−0.650
6H-4	31	48.71	49.81	1.2670	3.33			1.86	0.915	71.04	71.04	10.7	1.232	−0.940
6H-4	51	48.91	50.01	1.2730	3.08			2.64	0.940	66.64	66.64	9.6	1.361	−0.750
6H-4	71	49.11	50.21	1.2800	3.08			6.26	1.006	52.57	52.57	3.1	0.880	−0.390
6H-4	91	49.31	50.41	1.2860	3.33			4.32	1.033	57.69	57.69	5.2	0.910	−0.540
6H-4	111	49.51	50.61	1.2920	3.33			3.48	0.985	66.14	66.14	4.8	1.005	−0.330
6H-4	131	49.71	50.81	1.2980	3.33			4.10	0.980	54.23	54.23	4.6	1.055	−0.870
6H-5	1	49.91	51.01	1.3040	3.33			5.44	1.056	57.48	57.48	1.5	0.513	−0.770
6H-5	21	50.11	51.21	1.3100	3.33			6.80	1.095	57.81	57.81	9.1	0.594	−0.610
6H-5	41	50.31	51.41	1.3160	3.33			6.24	1.094	56.35	56.35	4.8	1.058	−0.480
6H-5	61	50.51	51.61	1.3220	3.33			6.96	1.124	50.22	50.22	2.8	1.082	−0.520
6H-5	81	50.71	51.81	1.3280	3.33			3.60	1.093	68.36	68.36	4.7	0.760	−1.320
6H-5	101	50.91	52.01	1.3340	3.33			3.26	1.019	67.91	67.91	7.1	0.801	−0.930
6H-5	121	51.11	52.21	1.3400	3.33			4.68	1.005	61.26	61.26	6.0	0.925	−0.660
6H-5	141	51.31	52.41	1.3460	3.33			5.44	1.091	57.34	57.34	3.6	0.929	−0.540
6H-6	11	51.51	52.61	1.3520	3.33			3.66	1.095	66.10	66.10	3.5	1.296	−0.440
6H-6	31	51.71	52.81	1.3580	3.08			4.58	1.079	57.21	57.21	4.9	1.381	−0.800
6H-6	51	51.91	53.01	1.3650	3.08			5.70	1.051	58.02	58.02	7.4	1.235	−0.140
6H-6	71	52.11	53.21	1.3710	3.33			6.24	1.077	53.90	53.90	2.8	1.222	−0.040
6H-6	91	52.31	53.41	1.3770	3.33			5.02	0.986	59.33	59.33	5.4	1.058	−0.510
6H-6	111	52.51	53.61	1.3830	3.33			4.60	1.004	55.51	55.51	3.3	1.595	−0.820
6H-6	131	52.71	53.81	1.3890	3.33			5.14	1.012	49.85	49.85	1.6	2.892	
6H-7	1	52.91	54.01	1.3950	3.33			4.92	[k]1.160	58.79	58.79	2.4	1.323	−1.160
6H-7	21	53.11	54.21	1.4010	3.33			6.52	[k]1.025	50.42	50.42	2.1	1.429	−0.560
6H-7	41	53.31	54.41	1.4070	3.33			[k]3.24	[k]0.985	68.33	[i]65.84	3.7	1.263	−1.140
6H-7	61	53.51	54.61	1.4130	3.33			[k]3.70	[k]1.039	60.07	[i]63.61	3.3	1.171	−0.560
			54.81	1.4190	3.33			[k]3.48	[k]1.073		[i]64.68			
			55.01	1.4250	3.33			[k]3.84	[k]1.100		[l]62.93			
			55.21	1.4310	3.33			[k]4.78	[k]1.052		[i]58.37			
			55.41	1.4370	3.08			[k]2.81	[k]1.005		[l]67.93			
			55.61	1.4440	3.08			[k]3.80	[k]0.951		[i]63.12			
			55.81	1.4500	3.33			[k]4.46	[k]1.100		[i]59.92			
			56.01	1.4560	3.33			[k]5.84	[k]0.971		[i]53.22			
7H-1	1	53.21	56.21	1.4620	3.33			[k]5.40	[k]1.025	54.34	[i]55.36	2.1	1.852	0.010
7H-1	21	53.41	56.41	1.4680	3.33			[k]5.02	0.951	51.91	[i]57.20	1.5	2.172	−1.070
7H-1	41	53.61	56.61	1.4740	3.33			4.92	1.011	51.90	[i]57.69	2.5	1.674	−0.920
7H-1	61	53.81	56.81	1.4800	3.33			6.96	1.023	45.76	45.76	2.9	1.127	−0.295
7H-1	81	54.01	57.01	1.4860	3.33			9.46	1.059	32.51	32.51	1.0	1.566	−0.560
7H-1	101	54.21	57.21	1.4920	3.33			7.20	1.098	49.66	49.66	1.7	1.208	−0.130
7H-1	121	54.41	57.41	1.4980	3.33			6.74	1.157	44.30	44.30	2.0	1.441	−0.450
7H-1	141	54.61	57.61	1.5040	3.33			5.06	1.082	57.95	57.95	4.0	1.144	−0.650
7H-2	11	54.81	57.81	1.5100	3.33			6.58	1.067	52.01	52.01	4.7	0.896	−0.460
7H-2	31	55.01	58.01	1.5160	3.08			5.86	1.124	61.26	61.26	4.2	0.887	−0.500
7H-2	51	55.21	58.21	1.5230	3.08			4.22	1.054	61.21	61.21	3.0	1.074	−1.250
7H-2	71	55.41	58.41	1.5290	3.33			3.76	1.036	61.86	61.86	4.2	0.862	−1.030
7H-2	91	55.61	58.61	1.5350	3.33			4.10	1.056	61.77	61.77	3.8	1.193	−0.670
7H-2	111	55.81	58.81	1.5410	3.33			7.04	1.133	46.89	46.89	4.2	0.820	−0.310
7H-2	131	56.01	59.01	1.5470	3.33			6.94	1.145	47.91	47.91	1.4	1.322	−0.390
7H-3	1	56.21	59.21	1.5530	3.33			4.90	1.170	51.13	51.13	1.0	1.344	−0.230
7H-3	21	56.41	59.41	1.5590	3.33			4.62	1.016	65.03	65.03	3.7	1.088	−0.990
7H-3	41	56.61	59.61	1.5650	3.33			5.66	0.986	52.76	52.76	1.4	1.491	
7H-3	61	56.81	59.81	1.5710	3.33			3.90	1.004	69.43	69.43	5.0	0.720	−1.285
7H-3	81	57.01	60.01	1.5770	3.33			8.24	1.106	41.42	41.42	2.8	1.995	−0.750
7H-3	101	57.21	60.21	1.5830	3.33			6.34	1.086	49.61	49.61	1.8	1.451	−0.820
7H-3	121	57.41	60.41	1.5890	3.33			3.90	1.047	56.93	56.93	1.9	1.799	−1.200

Appendix (continued).

Core, section	Section depth (cm)	ODP depth (m)	Composite[a] depth (m)	Ship[b] age (m.y.)	Ship sed. rate (cm/k.y.)	Isotope[c] age (m.y.)	Isotope sed. rate (cm/k.y.)	Composite[d] susceptibility (10^{-6}cgs)	Composite[e] density (g/cm^3)	$CaCO_3$ (%)	Composite[f] $CaCO_3$ (%)	>150 μm (%)	C-org (%)	$\delta^{18}O$ (‰)
7H-3	141	57.61	60.61	1.5950	3.08			2.56	1.025	65.65	65.65	2.3	1.401	
7H-4	11	57.81	60.81	1.6020	3.08			2.48	0.988	64.73	64.73	1.8	1.553	−0.920
7H-4	31	58.01	61.01	1.6080	3.33			[k]3.10	0.907	65.97	65.97	3.0	1.111	−0.820
7H-4	51	58.21	61.21	1.6140	3.33			[k]3.90	1.012	62.80	62.80	4.4	1.196	
7H-4	71	58.41	61.41	1.6200	3.33			[k]5.74	1.075	59.75	59.75	1.8	1.777	−0.430
7H-4	91	58.61	61.61	1.6260	3.33			[k]3.86	1.114	51.68	51.68	0.9	2.295	
7H-4	11	58.81	61.81	1.6320	3.33			[k]3.66	1.048	60.26	60.26	0.8	1.829	
7H-4	131	59.01	62.01	1.6380	3.33			[k]3.46	1.027	61.23	61.23	2.5	1.459	−1.250
7H-5	1	59.21	62.21	1.6440	3.33			4.38	1.205	61.27	61.27	4.8	0.951	−0.645
7H-5	21	59.41	62.41	1.6500	3.33			5.88	1.157	57.03	57.03	1.6	1.200	−0.370
7H-5	41	59.61	62.61	1.6560	3.33			3.60	1.104	68.87	68.87	1.4	1.235	−0.740
7H-5	61	59.81	62.81	1.6620	3.33			2.62	1.054	71.64	71.64	2.5	1.430	−1.130
7H-5	81	60.01	63.01	1.6680	3.33			2.62	1.015	71.54	71.54	2.8	1.290	
7H-5	101	60.21	63.21	1.6740	3.33			5.20	1.071	55.96	55.96	0.9	1.406	−1.160
7H-5	121	60.41	63.41	1.6800	3.08			4.90	1.149	58.08	58.08	1.2	1.727	−0.410
7H-5	141	60.61	63.61	1.6870	3.08			4.38	1.015	56.76	56.76	0.9	1.978	−0.540
7H-6	11	60.81	63.81	1.6930	3.33			2.00	1.131	75.13	75.13	1.8	1.436	
7H-6	31	61.01	64.01	1.6990	3.33			2.42	1.042	68.19	68.19	1.4	1.528	
7H-6	51	61.21	64.21	1.7050	3.33			2.34	1.012	66.64	66.64	2.0	2.059	−0.420
7H-6	71	61.41	64.41	1.7110	3.33			2.72	1.083	68.11	68.11	2.8	1.886	−0.610
7H-6	91	61.61	64.61	1.7170	3.33			2.78	1.063	65.88	65.88	2.4	1.665	−0.920
7H-6	111	61.81	64.81	1.7230	3.33			2.56	0.981	64.60	64.60	1.7	2.288	−0.950
7H-6	131	62.01	65.01	1.7290	3.33			4.66	1.090	58.72	58.72	1.4	1.876	−0.270
7H-7	1	62.21	65.21	1.7350	3.33			5.14	1.105	54.08	54.08	1.7	1.628	−0.770
7H-7	21	62.41	65.41	1.7410	3.33			5.58	[k]1.083	60.43	60.43	2.7	1.560	−0.310
7H-7	41	62.61	65.61	1.7470	3.33			7.68	[k]1.160	45.84	45.84	0.5	2.452	−0.310
7H-7	61	62.81	65.81	1.7530	3.21			4.00	[k]1.073	69.91	69.91	1.9	1.391	
			66.06	1.7610	3.21			[k]5.88	[k]1.133		[i]56.93			
			66.26	1.7670	3.33			[k]4.40	[k]1.046		[i]62.86			
8H-1	1	62.91	66.46	1.7730	3.33			[k]7.62	1.147	57.08	57.08	1.8	2.183	−0.760
8H-1	21	63.11	66.66	1.7790	3.33			4.18	1.008	63.49	63.49		2.454	
8H-1	41	63.31	66.86	1.7850	3.33			1.30	1.094	81.46	81.46	3.4	1.772	−1.140
8H-1	61	63.51	67.06	1.7910	3.33			2.16	1.097	76.45	76.45	3.4	1.476	−0.800
8H-1	81	63.71	67.26	1.7970	3.08			3.50	1.113	66.37	66.37	2.1	1.394	−0.330
8H-1	101	63.91	67.46	1.8040	3.08			3.36	1.110	68.60	68.60	1.1	1.824	−0.520
8H-1	121	64.11	67.66	1.8100	3.33			2.86	1.033	70.53	70.53	1.2	1.860	−0.690
8H-1	141	64.31	67.86	1.8160	3.33			2.38	1.042	72.51	72.51	2.6	1.283	−0.220
8H-2	11	64.51	68.06	1.8220	3.33			3.58	1.145	63.29	63.29	2.0	1.425	−0.350
8H-2	31	64.71	68.26	1.8280	3.33			3.08	1.058	71.57	71.57	1.7	1.425	−0.180
8H-2	51	64.91	68.46	1.8340	3.33			3.52	1.048	69.37	69.37	1.0	1.723	−0.340
8H-2	71	65.11	68.66	1.8400	3.33			3.98	1.033	63.95	63.95	0.9	1.950	
8H-2	91	65.31	68.86	1.8460	3.33			3.92	1.062	60.53	60.53	1.4	1.372	
8H-2	111	65.51	69.06	1.8520	3.33			1.40	1.160	80.93	80.93	3.8	1.758	−0.860
8H-2	131	65.71	69.26	1.8580	3.33			5.06	1.054	70.38	70.38	1.3	0.954	−0.740
8H-3	1	65.91	69.46	1.8640	3.33			6.14	1.152	67.89	67.89	2.3	1.594	
8H-3	21	66.11	69.66	1.8700	3.33			3.40	1.055	52.33	52.33	0.6	1.756	[j]−0.480
8H-3	41	66.31	69.86	1.8760	3.08			4.62	1.036	62.87	62.87	3.4	1.907	−0.780
8H-3	61	66.51	70.06	1.8830	3.08			4.90	0.990	56.04	56.04	1.6	1.737	−0.510
8H-3	81	66.71	70.26	1.8890	3.33			2.34	1.019	68.69	68.69	3.0	1.885	−0.940
8H-3	101	66.91	70.46	1.8950	3.33			3.70	1.038	69.06	69.06	6.5	1.372	−0.850
8H-3	121	67.11	70.66	1.9010	3.33			4.70	1.064	61.21	61.21	1.2	1.933	−0.300
8H-3	141	67.31	70.86	1.9070	3.33			4.84	1.144	57.77	57.77	0.9	1.525	
8H-4	11	67.51	71.06	1.9130	3.33			2.48	1.002	74.25	74.25	1.9	1.930	
8H-4	31	67.71	71.26	1.9190	3.33			2.16	0.961	73.61	73.61	2.5	1.774	−0.700
8H-4	51	67.91	71.46	1.9250	3.33			2.74	1.021	69.11	69.11	2.9	1.872	−0.730
8H-4	71	68.11	71.66	1.9310	3.33			2.66	1.081	66.53	66.53	1.3	1.962	−0.610
8H-4	91	68.31	71.86	1.9370	3.33			3.12	1.066	66.89	66.89	2.4	1.923	−0.520
8H-4	111	68.51	72.06	1.9430	3.33			4.08	1.083	62.83	62.83	1.8	2.311	−0.800
8H-4	131	68.71	72.26	1.9490	3.33			5.94	1.176	54.13	54.13	1.2	1.642	−0.300
8H-5	1	68.91	72.46	1.9550	3.33			3.16	1.112	68.44	68.44	3.4	1.613	−0.310
8H-5	21	69.11	72.66	1.9610	3.08			2.62	1.137	72.89	72.89	2.3	1.681	−0.820
8H-5	41	69.31	72.86	1.9680	3.08			4.04	1.066	62.38	62.38	0.9	1.827	−0.880
8H-5	61	69.51	73.06	1.9740	3.33			3.10	1.025	65.93	65.93	2.0	2.296	−1.060
8H-5	81	69.71	73.26	1.9800	3.33			5.52	1.093	59.35	59.35	2.8		−0.490
8H-5	101	69.91	73.46	1.9860	3.33			6.78	1.178	52.82	52.82	0.9	1.321	−0.720
8H-5	121	70.11	73.66	1.9920	3.33			3.24	1.060	68.84	68.84	2.5	1.284	−1.010
8H-5	141	70.31	73.86	1.9980	3.33			1.90	1.117	73.86	73.86	4.2	1.306	−1.010
8H-6	11	70.51	74.06	2.0040	3.33			2.50	1.071	70.67	70.67	2.6	1.596	
8H-6	31	70.71	74.26	2.0100	3.33			2.98	1.157	72.10	72.10	3.4	1.002	−0.470
8H-6	51	70.91	74.46	2.0160	3.33			2.80	1.083	74.74	74.74	3.0	1.197	−0.260
8H-6	71	71.11	74.66	2.0220	3.33			2.10	1.116	73.28	73.28	2.5	1.225	−0.430
8H-6	91	71.31	74.86	2.0280	3.33			1.58	1.095	75.95	75.95	2.6	1.490	−0.780
8H-6	111	71.51	75.06	2.0340	3.33			1.42	1.083	77.14	77.14	7.2	1.446	−0.560
8H-6	131	71.71	75.26	2.0400	3.08			1.50	1.140	78.06	78.06	2.4	1.396	−0.520
8H-7	1	71.91	75.46	2.0470	3.08			1.46	[k]1.086	76.87	76.87	2.5	1.288	−0.750
8H-7	21	72.11	75.66	2.0530	3.33			1.98	[k]1.012	72.29	72.29	1.9	1.135	−0.910

Appendix (continued).

Core, section	Section depth (cm)	ODP depth (m)	Composite[a] depth (m)	Ship[b] age (m.y.)	Ship sed. rate (cm/k.y.)	Isotope[c] age (m.y.)	Isotope sed. rate (cm/k.y.)	Composite[d] susceptibility (10^{-6}cgs)	Composite[e] density (g/cm^3)	$CaCO_3$ (%)	Composite[f] $CaCO_3$ (%)	>150 μm (%)	C-org (%)	$\delta^{18}O$ (‰)
8H-7	41	72.31	75.86	2.0590	3.33			1.40	[k]1.025	76.03	76.03	3.1	1.294	−0.990
8H-7	61	72.51	76.06	2.0650	3.33			1.02	[k]1.052	78.84	78.84	3.8	1.257	−0.860
721B			76.26	2.0710	3.33			[k]0.70	[k]1.025		[i]77.41			
721B			76.46	2.0770	3.33			[k]0.72	[k]1.005		[i]77.32			
721B			76.66	2.0830	3.33			[k]1.46	[k]1.086		[i]74.29			
9H-1	1	72.51	76.76	2.0860	3.33			[k]3.72	[k]1.093	58.09	[i]65.01	0.7	1.749	−0.360
9H-1	21	72.71	76.96	2.0920	3.33			3.50	[k]1.133	69.84	[i]65.91	2.8	1.594	
9H-1	41	72.91	77.16	2.0980	3.33			3.06	[k]1.046	66.25	66.25	2.0	1.624	
9H-1	61	73.11	77.36	2.1040	3.33			4.00	1.035	63.74	63.74	2.4	1.497	−0.455
9H-1	81	73.31	77.56	2.1100	3.33			3.90	1.059	63.99	63.99		1.703	
9H-1	101	73.51	77.76	2.1160	3.33			2.90	1.016	65.54	65.54	1.7	1.924	−0.800
9H-1	121	73.71	77.96	2.1220	3.08			1.80	1.085	70.87	70.87	2.6	1.744	−1.090
9H-1	141	73.91	78.16	2.1290	3.08			1.04	0.954	66.09	66.09	1.7	1.489	−0.940
9H-2	11	74.11	78.36	2.1350	3.33			1.20	0.893	70.96	70.96	3.4	1.493	−0.935
9H-2	31	74.31	78.56	2.1410	3.33			2.26	0.993	68.19	68.19	4.7	1.506	−0.710
9H-2	51	74.51	78.76	2.1470	3.33			4.32	1.070	60.69	60.69	3.2	1.315	0.200
9H-2	71	74.71	78.96	2.1530	3.33			3.84	1.035	62.90	62.90	1.0	1.692	
9H-2	91	74.91	79.16	2.1590	3.33			2.74	1.118	63.68	63.68	4.9	1.524	−0.290
9H-2	111	75.11	79.36	2.1650	3.33			1.52	1.066	71.83	71.83	3.7	1.341	−0.750
9H-2	131	75.31	79.56	2.1710	3.33			1.52	1.069	69.35	69.35	3.7	2.465	−0.640
9H-3	1	75.51	79.76	2.1770	3.33			2.90	1.006	64.81	64.81	3.6	2.044	−0.620
9H-3	21	75.71	79.96	2.1830	3.33			4.34	1.035	57.73	57.73	4.9	1.950	
9H-3	41	75.91	80.16	2.1890	3.33			4.34	1.117	58.49	58.49	1.4	1.761	−0.530
9H-3	61	76.11	80.36	2.1950	3.33			3.68	1.023	63.98	63.98	4.3	1.768	−0.450
9H-3	81	76.31	80.56	2.2010	3.08			4.44	1.012	60.26	60.26	3.1	1.235	−0.200
9H-3	101	76.51	80.76	2.2080	3.08			7.06	1.132	45.50	45.50	1.0	1.947	−0.940
9H-3	121	76.71	80.96	2.2140	3.33			2.12	1.105	71.59	71.59	0.8	2.027	−1.350
9H-3	141	76.91	81.16	2.2200	3.33			3.42	1.075	60.88	60.88	1.5	1.713	
9H-4	11	77.11	81.36	2.2260	3.33			5.32	0.980	50.68	50.68	1.2	2.116	
9H-4	31	77.31	81.56	2.2320	3.33			5.76	1.077	0.06	55.65	1.8	1.712	−0.880
9H-4	51	77.51	81.76	2.2380	3.33			5.84	1.029	47.65	47.65	1.1		−1.200
9H-4	71	77.71	81.96	2.2440	3.33			1.54	1.128	76.86	76.86	5.1	1.469	−1.243
9H-4	91	77.91	82.16	2.2500	3.33			4.26	1.001	56.75	56.75	1.8	1.931	−0.810
9H-4	111	78.11	82.36	2.2560	3.33			5.24	1.021	52.20	52.20	1.3	1.680	−0.080
9H-4	131	78.31	82.56	2.2620	3.33			2.42	1.075	71.11	71.11	1.7	1.754	−0.950
9H-5	1	78.51	82.76	2.2680	3.33			2.58	1.006	60.21	60.21	2.0	1.919	−0.820
9H-5	21	78.71	82.96	2.2740	3.33			3.66	1.056	65.00	65.00	1.8	1.654	−1.240
9H-5	41	78.91	83.16	2.2800	3.08			1.52	1.015	79.02	79.02	3.0	2.719	−0.820
9H-5	61	79.11	83.36	2.2870	3.08			3.40	1.054	65.69	65.69	2.8	1.728	−1.190
9H-5	81	79.31	83.56	2.2930	3.33			6.88	1.052	47.57	47.57	0.9	2.118	
9H-5	101	79.51	83.76	2.2990	3.33			2.76	1.063	68.96	68.96	1.6	2.101	−1.470
9H-5	121	79.71	83.96	2.3050	3.33			4.46	0.950	55.36	55.36	1.2	2.739	−1.140
9H-5	141	79.91	84.16	2.3110	3.33			3.88	1.043	63.86	63.86	1.1	2.284	−0.890
9H-6	11	80.11	84.36	2.3170	3.33			4.64	1.060	58.73	58.73	2.4	1.662	−0.560
9H-6	31	80.31	84.56	2.3230	3.33			5.42	1.164	53.23	53.23	1.1	2.636	
9H-6	51	80.51	84.76	2.3290	3.33			1.06	1.025	81.37	81.37	2.8	2.575	−0.955
9H-6	71	80.71	84.96	2.3350	3.33			2.82	1.019	65.92	65.92	1.8	3.194	
9H-6	91	80.91	85.16	2.3410	3.33			5.70	1.136	50.36	50.36	0.5	2.559	
9H-6	111	81.11	85.36	2.3470	3.33			4.58	0.963	52.61	52.61	0.4	3.741	
9H-6	131	81.31	85.56	2.3530	3.33			2.14	1.052	67.00	67.00	1.2	2.697	
9H-7	1	81.51	85.76	2.3590	3.08			2.92	[k]0.911	64.86	64.86	0.8	2.730	
9H-7	21	81.71	85.96	2.3660	3.08			2.96	[k]1.012	62.52	62.52	0.7	2.506	
9H-7	41	81.91	86.16	2.3720	3.33			3.30	[k]1.086	62.24	62.24	0.7	2.256	−0.720
9H-7	61	82.11	86.36	2.3780	3.46			2.02	[k]1.052	71.99	71.99	1.6	2.382	−1.210
			86.61	2.3850	3.46			[k]3.76	[k]0.998		[i]60.59			
			86.81	2.3910	3.33			[k]3.04	[k]0.958		[i]65.03			
			87.01	2.3970	3.33			[k]2.52	[k]0.965		[i]68.24			
			87.21	2.4030	3.08			[k]2.84	[k]0.971		[i]66.27			
			87.41	2.4100	3.08			[k]2.62	[k]0.944		[i]67.63			
10H-1	1	82.71	87.61	2.4160	3.33			[k]1.50	[k]1.019	59.06	[i]74.54	1.2	2.288	−1.040
10H-1	21	82.91	87.81	2.4220	3.33			2.76	0.985	69.29	[i]66.76	1.0	2.908	
10H-1	41	83.11	88.01	2.4280	3.33			2.96	1.064	68.84	[i]65.53	1.2	2.986	
10H-1	61	83.31	88.21	2.4340	3.33			2.58	0.993	68.65	68.65	0.9	2.375	
10H-1	81	83.51	88.41	2.4400	3.33			1.92	0.944	72.01	72.01	0.9	2.233	−1.110
10H-1	101	83.71	88.61	2.4460	3.33			2.44	0.954	69.09	69.09	0.8	2.769	−1.220
10H-1	121	83.91	88.81	2.4520	3.33			3.46	1.024	66.94	66.94	1.6	2.720	−1.210
10H-1	141	84.11	89.01	2.4580	3.33			3.58	0.975	60.70	60.70	0.8	3.112	
10H-2	11	84.31	89.21	2.4640	3.33			3.12	0.891	64.61	64.61	1.0	2.528	
10H-2	31	84.51	89.41	2.4700	2.67			3.10	0.993	66.55	66.55	1.1	2.791	
10H-2	51	84.71	89.61	2.4790	2.22			4.20	0.944	57.04	57.04	1.0	3.142	
10H-2	71	84.91	89.81	2.4880	2.22			3.62	1.009	61.29	61.29	0.8	2.649	
10H-2	91	85.11	90.01	2.4970	2.35			3.48	0.934	59.38	59.38	0.5	3.362	
10H-2	111	85.31	90.21	2.5050	2.35			4.16	0.998	58.19	58.19	0.6	2.939	
10H-2	131	85.51	90.41	2.5140	2.22			2.04	0.951	70.57	70.57	0.7	2.631	
10H-3	1	85.71	90.61	2.5230	2.35			4.16	1.029	59.74	59.74	0.7	3.271	
10H-3	21	85.91	90.81	2.5310	2.35			7.24	1.042	45.59	45.59	0.3	4.208	

Appendix (continued).

Core, section	Section depth (cm)	ODP depth (m)	Composite[a] depth (m)	Ship[b] age (m.y.)	Ship sed. rate (cm/k.y.)	Isotope[c] age (m.y.)	Isotope sed. rate (cm/k.y.)	Composite[d] susceptibility (10^{-6}cgs)	Composite[e] density (g/cm^3)	$CaCO_3$ (%)	Composite[f] $CaCO_3$ (%)	>150 μm (%)	C-org (%)	$\delta^{18}O$ (‰)
10H-3	41	86.11	91.01	2.5400	2.22			4.78	0.923	56.40	56.40	0.4	2.478	
10H-3	61	86.31	91.21	2.5490	2.35			3.06	0.997	69.54	69.54	1.1	1.816	
10H-3	81	86.51	91.41	2.5570	2.35			4.34	0.918	56.74	56.74	0.4	2.228	
10H-3	101	86.71	91.61	2.5660	2.22			5.12	0.984	53.88	53.88	0.2	3.005	
10H-3	121	86.91	91.81	2.5750	2.35			2.84	0.978	73.40	73.40	1.1	1.341	
10H-3	141	87.11	92.01	2.5830	2.35			4.28	0.955	57.83	57.83	0.4	2.799	
10H-4	11	87.31	92.21	2.5920	2.22			4.64	0.966	56.03	56.03	0.5		
10H-4	31	87.51	92.41	2.6010	2.35			2.40	0.998	73.87	73.87	1.1		
10H-4	51	87.71	92.61	2.6090	2.35			3.56	0.989	65.40	65.40	0.5		
10H-4	71	87.91	92.81	2.6180	2.22			4.68	1.006	0.06	58.50	0.4		
10H-4	91	88.11	93.01	2.6270	2.22			4.42	0.997	60.32	60.32	0.4		
10H-4	111	88.31	93.21	2.6360	2.35			4.00	1.040	61.66	61.66	0.5	2.758	
10H-4	131	88.51	93.41	2.6440	2.35			6.60	1.028	48.46	48.46	0.3	3.393	
10H-5	1	88.71	93.61	2.6530	2.22			6.36	0.878	49.66	49.66	0.3	2.660	
10H-5	21	88.91	93.81	2.6620	2.35			2.72	1.086	70.84	70.84	1.3	1.904	
10H-5	41	89.11	94.01	2.6700	2.35			4.72	1.086	64.94	64.94	0.8	2.444	
10H-5	61	89.31	94.21	2.6790	2.22			7.88	1.058	40.31	40.31	0.2	3.771	
10H-5	81	89.51	94.41	2.6880	2.35			6.22	1.113	53.87	53.87	0.5	1.946	
10H-5	101	89.71	94.61	2.6960	2.35			3.62	1.056	65.73	65.73	0.7	2.485	
10H-5	121	89.91	94.81	2.7050	2.22			4.34	1.005	55.75	55.75	0.4	3.760	
10H-5	141	90.11	95.01	2.7140	2.35			4.00	1.005	62.66	62.66	0.5	1.532	
10H-6	11	90.31	95.21	2.7220	2.35			1.86	1.000	76.63	76.63	2.0	1.350	
10H-6	31	90.51	95.41	2.7310	2.22			2.88	1.089	70.38	70.38	0.6	2.071	
10H-6	51	90.71	95.61	2.7400	2.22			4.38	1.093	61.05	61.05	0.5	2.773	
10H-6	71	90.91	95.81	2.7490	2.35			4.50	1.082	60.83	60.83	0.2	2.842	
10H-6	91	91.11	96.01	2.7570	2.35			3.44	0.984	65.55	65.55	0.5	2.238	
10H-6	111	91.31	96.21	2.7660	2.22			2.94	1.039	74.35	74.35	2.1	1.359	
10H-6	131	91.51	96.41	2.7750	2.35			3.98	1.081	64.93	64.93	0.5	2.430	
10H-7	1	91.71	96.61	2.7830	2.35			4.56	[k]1.005	58.54	58.54	0.6	2.994	
10H-7	21	91.91	96.81	2.7920	2.22			3.84	[k]0.904	65.30	65.30	0.7	2.402	
10H-7	41	92.11	97.01	2.8010	2.35			4.36	[k]0.911	64.58	64.58	0.8	2.177	
10H-7	61	92.31	97.21	2.8090	2.37			6.16	[k]0.944	46.58	46.58	0.2	4.727	
11X-1	1	91.91	97.46	2.8200	2.25			[k]3.06	[k]1.093	62.34	62.34	1.1	1.724	
11X-1	21	92.11	97.66	2.8290	2.22			[k]3.66	[k]1.039	75.83	75.83	2.1	1.605	
11X-1	41	92.31	97.86	2.8380	2.35			[h]2.40	1.048	74.62	74.62	1.7	1.130	
11X-1	61	92.51	98.06	2.8460	2.35			[h]2.60	0.912	69.74	69.74	0.6	2.221	
11X-1	81	92.71	98.26	2.8550	2.22			[h]2.64	0.965	69.64	69.64	0.8	1.932	
11X-1	101	92.91	98.46	2.8640	2.35			[h]3.12	0.977	69.39	69.39	0.8	1.729	
11X-1	121	93.11	98.66	2.8720	2.35			[h]4.08	0.905	69.22	69.22	0.5	2.434	
11X-1	141	93.31	98.86	2.8810	2.22			[h]3.64	0.915	57.24	57.24	0.4	2.859	
11X-2	11	93.51	99.06	2.8900	2.35			[h]4.12	0.907	62.80	62.80	0.7	2.135	
11X-2	31	93.71	99.26	2.8980	2.35			3.86	0.943	71.50	71.50	1.4	1.016	
11X-2	51	93.91	99.46	2.9070	2.22			4.44	0.971	65.65	65.65	0.5	2.352	
11X-2	71	94.11	99.66	2.9160	2.22			3.96	0.935	61.57	61.57	1.0	1.598	−0.830
11X-2	91	94.31	99.86	2.9250	2.59			4.38	1.036	62.88	62.88	0.5	1.982	
11X-2	111	94.51	100.06	2.9330	2.59			3.98	0.951	60.67	60.67	0.5	2.871	
11X-2	131	94.71	100.26	2.9420	2.22			3.34	0.911	66.82	66.82	0.4	3.389	
11X-3	1	94.91	100.46	2.9510	2.35			4.74	0.820	56.14	56.14	0.3	4.376	
11X-3	21	95.11	100.66	2.9590	2.35			3.50	0.853	67.52	67.52	0.3	3.052	
11X-3	41	95.31	100.86	2.9680	2.22			3.68	0.881	71.67	71.67	0.7	1.447	
11X-3	61	95.51	101.06	2.9770	2.35			3.88	0.969	64.12	64.12	0.5	2.491	
11X-3	81	95.71	101.26	2.9850	2.35			3.26	0.911	67.19	67.19	0.6	1.947	
11X-3	101	95.91	101.46	2.9940	2.22			4.72	1.035	57.66	57.66	0.5	1.926	
11X-3	121	96.11	101.66	3.0030	2.35			2.98	0.857	64.43	64.43	2.3	1.085	−1.370
11X-3	141	96.31	101.86	3.0110	2.35			3.82	1.063	63.72	63.72	1.8	1.322	−1.540
11X-4	11	96.51	102.06	3.0200	2.22			4.82	0.971	59.36	59.36	1.1	1.041	[j]−0.900
11X-4	31	96.71	102.26	3.0290	2.22			2.36	1.104	75.61	75.61	1.5	0.984	−1.450
11X-4	51	96.91	102.46	3.0380	2.35			2.36	1.016	74.79	74.79	1.1	1.966	−2.080
11X-4	71	97.11	102.66	3.0460	2.35			3.26	1.023	66.95	66.95	0.8	1.792	−1.440
11X-4	91	97.31	102.86	3.0550	2.22			2.80	1.028	69.88	69.88	1.2	1.218	−1.390
11X-4	111	97.51	103.06	3.0640	2.11			2.54	1.052	67.68	[i]72.80	1.5	1.025	−1.760
			103.31	3.0740	2.11			[k]3.22	[k]0.938		[i]68.55			
			103.51	3.0830	2.22			[k]3.88	[k]0.958		[i]64.42			
			103.71	3.0920	2.22			[k]2.66	[k]1.005		[i]72.05			
			103.91	3.1010	2.35			[k]3.05	[k]1.019		[i]69.61			
			104.11	3.1090	2.35			[k]4.04	[k]0.958		[i]63.42			
			104.31	3.1180	2.22			[k]3.20	[k]0.951		[i]68.67			
			104.51	3.1270	2.35			[k]1.40	[k]0.998		[i]79.93			
			104.71	3.1350	2.35			[k]1.52	[k]0.951		[i]79.18			
			104.91	3.1440	2.22			[k]2.04	[k]0.918		[i]75.93			
			105.11	3.1530	2.35			[k]3.10	[k]0.998		[i]69.30			
			105.31	3.1610	2.35			[k]3.12	[k]0.971		[i]69.17			
			105.51	3.1700	2.22			[k]2.74	[k]0.998		[i]71.55			
			105.71	3.1790	2.35			[h]3.10	[h]0.971		[i]69.30			
			105.91	3.1870	2.35			[h]4.76	[h]1.012		[i]58.91			
			106.11	3.1960	2.22			[h]3.12	[h]0.985		[i]69.17			

Appendix (continued).

Core, section	Section depth (cm)	ODP depth (m)	Composite[a] depth (m)	Ship[b] age (m.y.)	Ship sed. rate (cm/k.y.)	Isotope[c] age (m.y.)	Isotope sed. rate (cm/k.y.)	Composite[d] susceptibility (10^{-6}cgs)	Composite[e] density (g/cm^3)	$CaCO_3$ (%)	Composite[f] $CaCO_3$ (%)	>150 μm (%)	C-org (%)	$\delta^{18}O$ (‰)
			106.31	3.2050	2.22			[h]2.24	[h]0.958		[i]74.68			
			106.51	3.2140	2.35			[h]4.34	[h]0.897		[i]61.54			
			106.71	3.2220	2.35			[h]3.50	[h]1.073		[i]66.79			
			106.91	3.2310	2.22			[h]2.96	[h]0.965		[i]70.17			
			107.11	3.2400	2.35			[h]3.02	[h]0.985		[i]69.80			
12X-1	1	101.51	107.31	3.2480	2.35			[h]1.18	[h]1.012	67.51	[i]81.31	2.2	1.192	−0.930
12X-1	21	101.71	107.51	3.2570	2.22			[h]2.42	1.028	72.85	[i]73.55	0.9	0.992	−0.940
12X-1	41	101.91	107.71	3.2660	2.35			[h]2.88	1.054	76.03	[i]70.67	1.8	1.031	−1.010
12X-1	61	102.11	107.91	3.2740	2.35			[h]1.94	1.069	73.16	[i]76.55	1.7	1.007	−0.970
12X-1	81	102.31	108.11	3.2830	2.22			[h]1.86	1.073	72.03	[i]77.05	1.3	1.064	−0.970
12X-1	101	102.51	108.31	3.2920	2.35			2.60	1.025	76.67	[i]72.42	2.5	0.868	−1.170
12X-1	121	102.71	108.51	3.3000	2.35			1.80	0.997	78.48	78.48	2.6	1.133	−1.505
12X-1	141	102.91	108.71	3.3090	2.22			2.20	1.060	75.43	75.43	2.5	0.957	−1.540
12X-2	11	103.11	108.91	3.3180	2.22			3.00	1.006	72.58	72.58	1.1	1.586	[j]−0.690
12X-2	31	103.31	109.11	3.3270	2.35			3.08	1.044	72.98	72.98	0.8	1.556	−1.100
12X-2	51	103.51	109.31	3.3350	2.35			2.32	1.093	74.02	74.02	2.6	1.754	−1.130
12X-2	71	103.71	109.51	3.3440	2.22			3.52	1.083	68.78	68.78	0.9	1.038	
12X-2	91	103.91	109.71	3.3530	2.35			4.60	1.081	61.21	61.21	0.7	1.380	
12X-2	111	104.11	109.91	3.3610	2.35			2.34	1.029	75.50	75.50	1.6	0.997	−1.300
12X-2	131	104.31	110.11	3.3700	2.22			1.32	1.087	79.84	79.84	2.3	1.008	−1.395
12X-3	1	104.51	110.31	3.3790	2.35			2.28	1.008	71.41	71.41	0.7	1.821	
12X-3	21	104.71	110.51	3.3870	2.35			2.96	1.058	72.38	72.38	2.2	1.523	
12X-3	41	104.91	110.71	3.3960	2.22			4.30	1.066	59.82	59.82	0.8	1.608	
12X-3	61	105.11	110.91	3.4050	2.35			1.40	1.017	73.86	73.86	3.2	0.833	−1.630
12X-3	81	105.31	111.11	3.4130	2.35			1.74	1.013	77.82	77.82	3.7	0.721	−1.265
12X-3	101	105.51	111.31	3.4220	2.22			3.68	1.059	62.41	62.41	1.2	0.627	

[a] Composite depth below seafloor based on Hole 722B data with patches from Holes 722A and 721B.
[b] Ages based on magnetic datums recognized in Hole 722B.
[c] Ages based on oxygen isotope chronostratigraphy of Imbrie et al. (1984) and Ruddiman et al. (1989).
[d] Composite magnetic susceptibility section with missing and suspect intervals obtained from Holes 722A and 721B with preference given to Hole 721B data. Original 5-cm-spaced data were sampled at a 20-cm spacing using linear interpolation.
[e] Composite dry bulk density data with missing data obtained from Holes 722A and 721B. See text for conversion of GRAPE data to dry bulk density. Original 1.8-cm-spaced GRAPE data were sampled at a 20-cm interval using linear interpolation.
[f] Composite $CaCO_3$ data for Hole 722B.
[g] Value divided by two when plotted.
[h] Spliced data from Hole 722A.
[i] Values derived from regression of magnetic susceptibility and 100 − $CaCO_3$ for 10 samples above and 10 below data gap. The value at 5.54 m is based on a regression of 6 samples above and 6 below 5.54 m.
[j] Sample generated low gas volumes during analysis. Data are suspect.
[k] Spliced data from Hole 721B.
[l] Concentrations at 24.91 and 25.31 m (ODP depth) switched to provide a match between 100 − $CaCO_3$ and magnetic susceptibility.